Axion dark matter and additional BSM aspects in an extended 2HDM setup

Giorgio Arcadi[1,2,*] and Sarif Khan[3,†]

[1]*Dipartimento di Scienze Matematiche e Informatiche, Scienze Fisiche e Scienze della Terra, Università degli Studi di Messina, Viale Ferdinando Stagno d'Alcontres 31, I-98166 Messina, Italy*
[2]*INFN Sezione di Catania, Via Santa Sofia 64, I-95123 Catania, Italy*
[3]*Institute for Theoretical Physics, Georg-August University Göttingen, Friedrich-Hund-Platz 1, Göttingen, D-37077 Germany*

(Received 25 February 2024; accepted 4 June 2024; published 8 July 2024)

We illustrate and discuss the phenomenology of a model featuring a two-Higgs doublet sector augmented by two $SU(2)$ singlet scalars. The gauge symmetry group is extended as well with a $U(1)_{L_\mu - L_\tau}$ component whose spontaneous breaking leads to the gauge boson which has an important effect in the muon $(g-2)$. A global PQ symmetry is introduced upon its breaking; we have the axion particle which is also dark matter (DM) in our work. In particular, we have focused on type-X and type-II 2HDM models and found out that $(g-2)$ cannot be explained only by the scalar sector for type-II 2HDM mainly due to stringent constraint from $b \to s\gamma$ resulted in $M_{H^\pm} > 800$ GeV. For type-II 2HDM, we can have axion coupling with the gluons which generates the axion potential and possible explanation for the strong CP problem. The proposed model accommodates neutrino masses via the type-I seesaw mechanism with an upper bound on the right-handed neutrino mass 1 GeV (1 TeV) for type-II (type-X) 2HDM due to the presence of Planck scale suppressed operators. Moreover, we also have additional scalars which affect the oblique parameters and hence the W-boson mass which leads us to explain the W-boson mass observed at the CDF-II detector. The most stringent constraints on the masses and quartic couplings come from the perturbativity and potential bound from the below conditions which leads to fine-tuning among the parameters in part of the parameter space. Finally, we discuss the possible detection prospects of the axion DM and the additional gauge boson.

DOI: 10.1103/PhysRevD.110.015011

I. INTRODUCTION

In the present work, we aim to address several drawbacks which are intact in pure Standard Model (SM) and demand beyond SM (BSM) physics to tackle them. With the progression of experiments, few important limitations within the SM have come to light, including the presence of dark matter (DM) [1], nonzero neutrino mass [2–4], disagreement between the theoretical and experimental values of the muon $(g-2)$ [5], and larger values of W-boson mass as confirmed by the CDF-II measurement [6]. Confirmation of DM's existence has been derived from several observations, notably evident in the flatness of the rotational curve [7], discrepancies in the center of masses of the visible sector compared to the total mass in the bullet cluster data [8], and the precise measurement of the DM quantity through cosmic microwave background data collected by the Planck satellite [9].

Axion is one of the most popular and best motivated proposals to address the DM puzzle. The existence of the axion is originally connected with the strong CP problem, namely the suppression of the following topological term in the QCD Lagrangian:

$$\mathcal{L}^{\theta}_{CP} = (\theta + \arg[\det(m_q)])\frac{g_s^2}{32\pi^2} G_{\mu\nu}\widetilde{G^{\mu\nu}}, \tag{1}$$

where g_s is the strong sector gauge coupling, m_q is the quark mass matrix, and $\widetilde{G^{\mu\nu}} = \epsilon^{\mu\nu\rho\sigma}G_{\rho\sigma}$ is the dual of the strong sector field strength tensor $G_{\mu\nu}$. The presence of this term explicitly breaks the parity symmetry, resulting in the generation of a nonzero electric dipole moment for the neutron (d_n), estimated around $d_n \sim 10^{-16}\bar{\theta}$ e cm [where $\bar{\theta} = \theta + \arg[\det(m_q)]$]. However, the current experimental limit, $d_n < 10^{-26}$ e cm, imposes a stringent constraint on the θ term, indicating $\bar{\theta} < 10^{-10}$ [10]. The remarkably small magnitude of $\bar{\theta}$ seems unnatural; given its nature as

*giorgio.arcadi@unime.it
†sarif.khan@uni-goettingen.de

an angular variable would typically be expected as $\mathcal{O}(1)$. The Peccei-Quinn mechanism [11–14] allows to set the $\bar{\theta}$ parameter via the introduction of an appropriate symmetry, with the axion being a pseudo-Goldstone boson associated to the latter. Observational constraints favor the axion to have extremely suppressed couplings with the ordinary matter which make it cosmologically stable and, hence, a potential DM candidate.

Another important limitation of the SM is represented by the origin of neutrino masses. In the SM, no mass terms are present of the neutrinos, as there are no right-handed counterparts to the left-handed neutrinos present in the $SU(2)$ lepton doublets. Oscillation data by many experiments [15–18] contradict the SM prediction as they require massive neutrinos, with sub-eV mass splittings, to be accounted for.

Another problem is the measurement of the muon $(g-2)$ which disagrees with the theoretical value measured by the SM [5] and the experimental observation [19]. The recent measurement of muon $(g-2)$ at FNAL disagrees with the SM value at 4.2σ. It is worth mentioning that the measurement of vacuum hadronic polarization contribution by different methods can decrease the disagreement. For example, the lattice calculation by the BMW collaboration [20] has reduced the anomaly down to 1.5σ. Moreover, the recent measurement of the $e^+e^- \to \pi^+\pi^-$ cross section at the CMD-III experiments [21] has also decreased the discrepancy between the theoretical and experimental values to 2.4σ. However, the lattice data and CMD-III data are not final and they also need to be confirmed before any conclusion. In this work, we have focused on explaining the disagreement between the muon $g-2$ values obtained theoretically from SM and at the FNAL experiment. There is also another drawback of SM in the measurement of the W-boson mass if we consider the CDF-II measurement [6]. The latter disagrees with the SM value by 7σ, hence, calling of an extra BSM contribution to the mass of the gauge boson.

In this work, we propose a model addressing the DM puzzle (via axion), the origin of neutrino masses as well as the observational hints summarized above. The model consists of an extended Higgs sector, made by two $SU(2)$ doublets and two complex scalar singlets, as well as an extended gauge group, with a spontaneously broken anomaly-free (via suitable charge assignments of the field) $U(1)_{L_\mu - L_\tau}$. The two complex scalar singlets provide additional pseudoscalar degrees of freedom which allow to provide a longitudinal component to the gauge boson of the new symmetry and, at the same time, to incorporate an axion field. Three right-handed neutrinos are, finally, present which allow to generate the SM neutrino masses via seesaw. Analogously to the conventional 2HDM, we have assumed *ad hoc* Z_2 symmetries, as well as specific assignations of the charges of the scalars under the new symmetry, to prevent tree-level flavor changing neutral current (FCNC) [22,23]. Interestingly, this combination of charge assignments and discrete symmetries resembles an accidental PQ symmetry [11–14]. This kind of possibility has been explored, e.g., in [24–28] and can be easily implemented in our work without impacting the phenomenology. It is worth mentioning that the additional discrete symmetries can be originated as residual symmetries when a gauge symmetry breaks as exhibited in Ref. [29]. Alternatively, one could consider explicitly introducing a global $U(1)_{\rm PQ}$ symmetry [30]. As is well known, however, global symmetries are expected to be broken by gravity [31–35].

In the present work due to the charge assignments, we have found that the axion field and right-handed neutrino masses originate from the same fields by its CP-odd component and vacuum expectation value (VEV), respectively. The axion and neutrino masses in 2HDM setup have been studied in [30,36] but our work is completely different. We have focused on the type-II and the type-X 2HDM model. As we will see later, in explaining the muon $(g-2)$ from type-II 2HDM, we need 100% contribution from the additional gauge boson because of the very tight constraint on the charged Higgs mass $M_{H^\pm} > 800$ GeV coming from the $b \to s\gamma$ measurement [37,38]. On the other hand, for type-X 2HDM, we can explain the muon $(g-2)$ from the Higgs sector as well in part of the region but the immediate drawback of type-X is that it cannot explain the strong CP problem in contrast to type-II 2HDM which cannot generate 100% muon $(g-2)$ only from the Higgs sector. In the case of neutrino mass, it does not distinguish the type-X and type-II 2HDM because the Dirac mass matrix depends on the Higgs doublet H_2 and right-handed neutrino masses depend on singlet scalars. As will be discussed later, to explain the $(g-2)$ we cannot choose the gauge coupling and gauge boson mass randomly which will impact the right-handed neutrino mass. Because of the dependence of a few elements in the right-handed neutrino mass matrix on Planck scale, we cannot get the right-handed (RH) neutrino masses above 1 GeV for the type-II but for type-X we can obtain any value for the right-handed neutrino mass. This hierarchy in RH neutrino masses for type-II 2HDM ensures the Dirac Yukawa coupling for the neutrinos can reach a maximal value $\mathcal{O}(10^{-8})$. For both type-II and type-X, we can explain the W-boson mass observed by the CDF-II detector and also the regions in S, T, U planes which are consistent with the SM predicted value of W-boson mass.

The rest of the paper is organized as follows. In Sec. II, we have explained the model in detail. The neutrino mass has been discussed in Sec. III and the axion DM study has been shown in Sec. IV. In Sec. V, we have discussed the muon $(g-2)$ followed by the allowed regions in Sec. VI. The W-boson mass has been studied in Sec. VII and finally we have presented our conclusion in Sec. VIII.

II. MODEL

In the present work, we have tried to explain the SM drawbacks, namely, the presence of dark matter, neutrino

mass, excess contribution in muon $(g-2)$ anomaly, strong CP problem, and extra contribution to W-boson mass as obtained by CDF-II data. In this context, we have tried to explain all of them from a common origin. In particular, we have considered axion DM in the context of the Dine–Fischler–Srednicki–Zhitnitsky (DFSZ) type axion model [39,40]. As we know, the CP-odd component present in 2HDM models cannot be axion DM because of many constraints; e.g., supernovae bound on axion decay constant [41]. Therefore, we extended the Higgs sector by two additional singlet scalars and an Abelian gauge symmetry. Among the extra two singlet scalars, one of them is neutral under the new Abelian gauge symmetry and the CP-odd component coming from it can be an axion DM and the other CP-odd component which is charged under Abelian gauge symmetry becomes the longitudinal component of additional gauge boson and impart mass to it. Moreover, we have introduced three right-handed neutrinos for generating the neutrino mass and their masses depend on the VEVs of the singlet scalars.

The particle content of the model, together with the charge assignments of the individual fields, is summarized in Tables I and II. In the tables, $H_{1,2}$ stands for the two $SU(2)$ doublets while $\phi_{1,2}$ are the new singlets. In principle, the additional $U(1)_{L_\mu - L_\tau}$ could represent any combination of the baryonic and leptonic charges of the fields which must obey the following gauge anomaly condition as described in Appendix A:

$$\sum_{i=1}^{3}(3b_i + b_i') = 0. \tag{2}$$

As can be seen from the above equation, by obeying the relation we can have many combinations for b_i, b_i' $(i = 1, 2, 3)$. In the present work, we have chosen $b_i = 0$, $b_1' = 0$, and $b_2' = -b_3' = 1$ which implies $L_\mu - L_\tau$ symmetry. As will be clarified below, this specific choice for the Abelian group is crucial to account for the generation of neutrino masses and to explain the $g-2$ anomaly. Furthermore, it can provide an accidental continuous global symmetry depending on the introduction of additional discrete symmetries. The model discussed in this work is described by the following Lagrangian:

$$\begin{aligned}\mathcal{L} &= \mathcal{L}_{\rm 2HDM} + \mathcal{L}_Y + \mathcal{L}_N \\ &\quad + \sum_{i=1,2}(D_\mu \phi_i)^\dagger (D^\mu \phi_i) - \mathcal{V}(H_1, H_2, \phi_1, \phi_2) \\ &\quad - \frac{1}{4} F^{i\alpha\beta}_{\mu\tau} F^{i}_{\mu\tau\alpha\beta},\end{aligned} \tag{3}$$

where $\mathcal{L}_{\rm 2HDM}$ consists of kinetic terms for all the fields for the pure 2HDM model [42], $\mathcal{L}_Y$ is the Yukawa terms associated with the SM quarks and leptons,

$$\mathcal{L}_Y = y^u_{ij}\bar{Q}^i_L \tilde{H}_2 u^j_R + y^d_{ij}\bar{Q}^i_L H_m d^j_R + y^l_{ij}\bar{L}^i_L H_n e^j_R + \text{H.c.}, \tag{4}$$

where $\tilde{\phi}_2 = i\sigma_2\phi_2^*$ and $m, n = 1, 2$. Depending on $m, n = 1, 2$ we can have four kinds of scenarios which are mentioned in Table III with the associated Peccei-Quinn charges for the quarks, leptons, and scalars. As pointed out in [22,23], the tree level FCNC can be forbidden if the same charge fermions get mass from the one scalar doublet. With this freedom, we can have four different types of combinations for the 2HDM model referred to as type-I, type-II, type-X, and type-Y, depending on the $H_{1,2}$ interaction with the quarks and leptons (shown in Table III). The four different types of 2HDM model can be achieved by introducing an additional global $U(1)_{\rm PQ}$ symmetry [11–14] with the charge assignment as shown in Table III and the same global symmetry will also help us in solving the strong CP problem. In this setup, the $U(1)_{\rm PQ}$ charges shown in Table III can introduce additional PQ-violating

TABLE I. Particle contents and their corresponding charges under the SM gauge group where i indicates the three generations for quarks and leptons.

Gauge group	Baryon fields			Lepton fields			Scalar fields			
	$Q^i_L = (u^i_L, d^i_L)^T$	u^i_R	d^i_R	$L^i_L = (\nu^i_L, e^i_L)^T$	e^i_R	N_i	H_1	H_2	ϕ_1	ϕ_2
$SU(2)_L$	2	1	1	2	1	1	2	2	1	1
$U(1)_Y$	1/6	2/3	−1/3	−1/2	−1	0	1/2	1/2	0	0

TABLE II. Charges of the particles under the new Abelian gauge group $U(1)_{L_\mu - L_\tau}$. The fermion doublets L^i_L and Q^i_L are defined in Table I.

Gauge group	Baryon fields			Lepton fields			Scalar fields			
	Q^i_L	u^i_R	d^i_R	(L^e_L, e_R, N_e)	(L^μ_L, μ_R, N_μ)	$(L^\tau_L, \tau_R, N_\tau)$	H_1	H_2	ϕ_1	ϕ_2
$U(1)_{L_\mu - L_\tau}$	b_i	b_i	b_i	b_1'	b_2'	b_3'	0	0	0	1

TABLE III. PQ charges of the particles under Peccei-Quinn symmetry $U(1)_{\rm PQ}$. The charges of L_L^i and Q_L^i are free parameters as defined by X_l and X_u, respectively, and can be chosen according to the purpose. Additionally, adhering to the conservation of global PQ symmetry at the Planck scale, the relationship between X_l and β within the neutrino sector Lagrangian, expressed as Eq. (5), is defined as $X_l = \frac{1}{2} - \cos^2\beta$.

Global	Classification		Scalar fields				Baryon fields			Lepton fields		
symmetry	Type	(m,n)	H_2	H_1	ϕ_1	ϕ_2	Q_L^i	u_R^i	d_R^i	L_L^j	e_R^j	N_R^j
$U(1)_{\rm PQ}$	I	(2,2)	$\cos^2\beta$	$-\sin^2\beta$	-1	0	X_u	$X_u+\cos^2\beta$	$X_u-\cos^2\beta$	X_l	$X_l-\cos^2\beta$	$X_l+\cos^2\beta$
	II	(1,1)	$\cos^2\beta$	$-\sin^2\beta$	-1	0	X_u	$X_u+\cos^2\beta$	$X_u+\sin^2\beta$	X_l	$X_l+\sin^2\beta$	$X_l+\cos^2\beta$
	X	(2,1)	$\cos^2\beta$	$-\sin^2\beta$	-1	0	X_u	$X_u+\cos^2\beta$	$X_u-\cos^2\beta$	X_l	$X_l+\sin^2\beta$	$X_l+\cos^2\beta$
	Y	(1,2)	$\cos^2\beta$	$-\sin^2\beta$	-1	0	X_u	$X_u+\cos^2\beta$	$X_u+\sin^2\beta$	X_l	$X_l-\cos^2\beta$	$X_l+\cos^2\beta$

terms at the Planck scale which may shift the axion potential because the global symmetry is not conserved up to the Planck scale [31–35]. This kind of situation can be evaded by introducing additional discrete symmetries which will make the PQ symmetry as the accidental global symmetry [24–28] and will forbid the extra PQ breaking terms up to the Planck scale or will have a minuscule impact at the axion potential. As indicated in Ref. [29], the extra discrete symmetries could manifest as residual symmetries arising from the spontaneous breaking of additional gauge symmetries, which remain protected from gravity-induced breaking. Among the four choices of the 2HDM model, we will see in the later part that type-II and type-Y 2HDM models can address the strong CP problem and the corresponding CP-odd scalar will become the axion DM. The other two choices, type-I and type-X, cannot solve the strong CP problem but still can produce axion-type DM by the misalignment mechanism [43–45]. The Lagrangian associated with the right-handed neutrinos takes the following form after obeying all the gauge symmetry and PQ symmetry:

$$\begin{aligned}\mathcal{L}_N = &\sum_{i=e,\mu,\tau}\frac{i}{2}\overline{N_L^i}\gamma^\mu D_\mu^N N_L^i - \sum_{i=e,\mu,\tau} y_{ii}\overline{L_i}\,\widetilde{H_2}\,N_i - \lambda_{ee}^N N_e N_e \phi_1 \\ &- \lambda_{e\mu} N_e N_\mu \phi_2^\dagger \frac{\phi_1}{M_{\rm pl}} \\ &- \lambda_{e\tau} N_e N_\tau \phi_2 \frac{\phi_1}{M_{\rm pl}} - \lambda_{\mu\tau}^N N_\mu N_\tau \phi_1 + \text{H.c.} \end{aligned} \tag{5}$$

In writing down the above interaction terms, we have chosen $X_l = \frac{1}{2} - \cos^2\beta$ and for other values of X_l we get different allowed interaction terms than above. It is worth highlighting from the above Lagrangian that the third and last terms with the superscript "N" in the Yukawa couplings are dimension-4 while the remaining terms associated with the right-handed neutrino masses are dimension-5 and suppressed by the Planck mass.

The potential consists of all the scalar fields after respecting all the symmetries in consideration have the following form:

$$\begin{aligned}\mathcal{V}(H_1,H_2,\phi_1,\phi_2) = &-\mu_{11}^2(H_1^\dagger H_1) - \mu_{22}^2(H_2^\dagger H_2) - \mu_{\phi_1}^2(\phi_1^\dagger\phi_1) - \mu_{\phi_2}^2(\phi_2^\dagger\phi_2) + \mu((H_1^\dagger H_2)\phi_1 + \text{H.c.}) \\ &+ \lambda_1(H_1^\dagger H_1)^2 + \lambda_2(H_2^\dagger H_2)^2 + \lambda_{\phi_1}(\phi_1^\dagger\phi_1)^2 + \lambda_{\phi_2}(\phi_2^\dagger\phi_2)^2 + \lambda_{12}(H_1^\dagger H_1)(H_2^\dagger H_2) \\ &+ \lambda_{12}'(H_1^\dagger H_2)(H_2^\dagger H_1) + \sum_{i,j=1,2}\lambda_{H_i\phi_j}(H_i^\dagger H_i)(\phi_j^\dagger\phi_j). \end{aligned} \tag{6}$$

The scalars H_1, H_2, ϕ_1, and ϕ_2 take the following form at the time of $U(1)_{L_\mu - L_\tau}$, PQ and electroweak symmetry, $SU(2)\times U(1)_Y$, breaking:

$$\begin{aligned} H_1 &= \begin{pmatrix} H_1^+ \\ \frac{v_1+H_1^0+iA_1^0}{\sqrt{2}}\end{pmatrix}, \qquad H_2 = \begin{pmatrix} H_2^+ \\ \frac{v_2+H_2^0+iA_2^0}{\sqrt{2}}\end{pmatrix}, \\ \phi_1 &= \left(\frac{v_{\phi_1}+\phi_1^0}{\sqrt{2}}\right)e^{i\frac{a_1}{v_{\phi_1}}}, \qquad \phi_2 = \left(\frac{v_{\phi_2}+\phi_2^0}{\sqrt{2}}\right)e^{i\frac{a_2}{v_{\phi_2}}}. \end{aligned} \tag{7}$$

The tadpole conditions which we obtain after demanding the first derivative of the potential with respect to the neutral components of the scalar fields are zero,

$$\mu_{11}^2 = \frac{2\lambda_1 v_1^3 + (\lambda_{12}+\lambda'_{12})v_1 v_2^2 + \sqrt{2}\mu v_2 v_{\phi_1} + v_1(\lambda_{H_1\phi_1} v_{\phi_1}^2 + \lambda_{H_1\phi_2} v_{\phi_2}^2)}{2v_1},$$
$$\mu_{22}^2 = \frac{2\lambda_2 v_2^3 + (\lambda_{12}+\lambda'_{12})v_2 v_1^2 + \sqrt{2}\mu v_1 v_{\phi_1} + v_2(\lambda_{H_2\phi_1} v_{\phi_1}^2 + \lambda_{H_2\phi_2} v_{\phi_2}^2)}{2v_2},$$
$$\mu_{\phi_1}^2 = \frac{\lambda_{H_1\phi_1} v_1^2 v_{\phi_1} + \lambda_{H_2\phi_1} v_2^2 v_{\phi_1} + \sqrt{2}\mu v_1 v_2 + 2\lambda_{\phi_1} v_{\phi_1}^3 + \lambda_{\phi_1\phi_2} v_{\phi_2}^2 v_{\phi_1}}{2v_{\phi_1}},$$
$$\mu_{\phi_2}^2 = \frac{\lambda_{H_1\phi_2} v_1^2 + \lambda_{H_2\phi_2} v_2^2 + 2\lambda_{\phi_2} v_{\phi_2}^2 + \lambda_{\phi_1\phi_2} v_{\phi_1}^2}{2}. \tag{8}$$

The neutral Higgs mass matrix in the basis $(H_1^0\, H_2^0\, \phi_2^0\, \phi_1^0)$ takes the following form:

$$\mathcal{L}^{\rm NH} = \begin{pmatrix} H_1^0 & H_2^0 & \phi_2^0 & \phi_1^0 \end{pmatrix} M_S^2 \begin{pmatrix} H_1^0 \\ H_2^0 \\ \phi_2^0 \\ \phi_1^0 \end{pmatrix}, \tag{9}$$

where the neutral Higgs mass matrix, M_S^2, takes the following form:

$$M_S^2 = \begin{pmatrix} 2\lambda_1 v_1^2 - \frac{\mu v_2 v_{\phi_1}}{\sqrt{2}v_1} & \left((\lambda_{12}+\lambda'_{12})v_1 v_2 + \frac{\mu v_{\phi_1}}{\sqrt{2}}\right) & \lambda_{H_1\phi_2} v_1 v_{\phi_2} & \left(\frac{\mu v_2}{\sqrt{2}} + \lambda_{H_1\phi_1} v_1 v_{\phi_1}\right) \\ \left((\lambda_{12}+\lambda'_{12})v_1 v_2 + \frac{\mu v_{\phi_1}}{\sqrt{2}}\right) & \left(2\lambda_2 v_2^2 - \frac{\mu v_1 v_{\phi_1}}{\sqrt{2}v_2}\right) & \lambda_{H_2\phi_2} v_2 v_{\phi_2} & \left(\frac{\mu v_1}{\sqrt{2}} + \lambda_{H_2\phi_1} v_2 v_{\phi_1}\right) \\ \lambda_{H_1\phi_2} v_1 v_{\phi_2} & \lambda_{H_2\phi_2} v_2 v_{\phi_2} & 2\lambda_{\phi_2} v_{\phi_2}^2 & \lambda_{\phi_1\phi_2} v_{\phi_1} v_{\phi_2} \\ \left(\frac{\mu v_2}{\sqrt{2}} + \lambda_{H_1\phi_1} v_1 v_{\phi_1}\right) & \left(\frac{\mu v_1}{\sqrt{2}} + \lambda_{H_2\phi_1} v_2 v_{\phi_1}\right) & \lambda_{\phi_1\phi_2} v_{\phi_1} v_{\phi_2} & -\frac{\mu v_1 v_2}{\sqrt{2}v_{\phi_1}} + 2\lambda_{\phi_1} v_{\phi_1}^2 \end{pmatrix}. \tag{10}$$

As will be discussed in Sec. IV, to have a negligible contribution to SM Higgs mass from the other heavy Higgses through higher loop order correction terms, we need to take $\lambda_{i\phi_1} \to 0$ $(i = H_1, H_2, \phi_2)$ and $\mu \ll 1$. This will make sure the M_S^2 mass matrix in the two block diagonal form as $(4\times 4) \simeq (3\times 3)\bigoplus(1\times 1)$. Therefore, we can relate the mass eigenbasis and flavor eigenbasis by the unitary matrix as

$$\begin{pmatrix} h_1 \\ h_2 \\ h_3 \\ \phi_1 \end{pmatrix} = \begin{pmatrix} R & 0 \\ 0 & 1 \end{pmatrix} \begin{pmatrix} H_1^0 \\ H_2^0 \\ \phi_2^0 \\ \phi_1^0 \end{pmatrix}, \tag{11}$$

where

$$R = \begin{pmatrix} c_1 c_2 & s_1 c_2 & s_2 \\ -c_1 s_2 s_3 - s_1 c_3 & c_1 c_3 - s_1 s_2 s_3 & c_2 s_3 \\ -c_1 s_2 c_3 + s_1 s_3 & -c_1 s_3 - s_1 s_2 c_3 & c_2 c_3 \end{pmatrix} \tag{12}$$

and $c_i = \cos\alpha_i$, $s_i = \sin\alpha_i$, and $-\frac{\pi}{2} \le \alpha_i \le \frac{\pi}{2}$ $(i = 1, 2, 3)$. The above diagonalization matrix can go back to the original 2HDM diagonalization matrix, with the singlet scalars completely decoupled from the two doublets, once we choose $\alpha_1 \to \alpha$ and $\alpha_{2,3} \to 0$.

The charged Higgs mass matrix in the basis $(H_1^+ H_2^+)$ takes the following form:

$$M_\pm^2 = \begin{pmatrix} -\frac{v_2}{2v_1}(\lambda'_{12} v_1 v_2 + \sqrt{2}\mu v_{\phi_1}) & \frac{\lambda'_{12} v_1 v_2 + \sqrt{2}\mu v_{\phi_1}}{2} \\ \frac{\lambda'_{12} v_1 v_2 + \sqrt{2}\mu v_{\phi_1}}{2} & -\frac{v_1}{2v_2}(\lambda'_{12} v_1 v_2 + \sqrt{2}\mu v_{\phi_1}) \end{pmatrix}. \tag{13}$$

Once we diagonalize Eq. (13) then we have two mass eigenstates $(H^\pm G^\pm)$ and they are related with the charged eigenbasis as

$$\begin{pmatrix} G^\pm \\ H^\pm \end{pmatrix} = \begin{pmatrix} \cos\beta & \sin\beta \\ -\sin\beta & \cos\beta \end{pmatrix} \begin{pmatrix} H_1^\pm \\ H_2^\pm \end{pmatrix}, \tag{14}$$

where $\tan\beta = \frac{v_2}{v_1}$. The mass of $H^\pm$ and $G^\pm$ in terms of the VEVs takes the following form:

$$M^2_{H^\pm} = -\frac{v_1^2+v_2^2}{2}\left(\lambda'_{12} + \frac{\sqrt{2}\mu v_{\phi_1}}{v_1 v_2}\right), \qquad M^2_{G^\pm} = 0. \quad (15)$$

Additionally, among the charged eigenstates, $G^\pm$ is the Goldstone boson which acts as the longitudinal mode of the $W^\pm$ gauge boson.

The CP-odd Higgs mass matrix in the basis $(A_1 A_2 a_1)$ takes the following form:

$$M^2_A = \begin{pmatrix} -\frac{\mu v_2 v_{\phi_1}}{\sqrt{2}v_1} & \frac{\mu v_{\phi_1}}{\sqrt{2}} & \frac{\mu v_2}{\sqrt{2}} \\ \frac{\mu v_{\phi_1}}{\sqrt{2}} & -\frac{\mu v_1 v_{\phi_1}}{\sqrt{2}v_2} & -\frac{\mu v_1}{\sqrt{2}} \\ \frac{\mu v_2}{\sqrt{2}} & -\frac{\mu v_1}{\sqrt{2}} & -\frac{\mu v_1 v_2}{\sqrt{2}v_{\phi_1}} \end{pmatrix}. \quad (16)$$

The CP-odd state A has the mass and, among the remaining two, G^0 is the Goldstone boson associated with the SM Z-boson and a is the axion field which will get mass during the QCD phase transition [46].

The 2HDM with a singlet scalar extension in the context of collider constraints has been studied in [47,48]. This work focuses on the other aspects of the 2HDM extension, namely dark matter, $(g-2)_\mu$, neutrino mass, and excess contribution in W-boson mass after adding two singlet scalars and an Abelian gauge symmetry. The parameters have been chosen in such a way that they comply with current collider constraints but will be in reach of future increased experimental sensitivity. The coupling of the Higgses with the SM gauge bosons can be expressed as

$$\mathcal{L}_{h_i VV} = i g_{\mu\nu} \lambda_{h_i VV} g^{\rm SM}_{VV}, \quad (20)$$

where $V = W^\pm, Z$, $\lambda_{h_i VV} = \cos\beta R_{i1} + \sin\beta R_{i2}$, and $g^{\rm SM}_{VV}$ is the SM Higgs coupling with the gauge bosons in pure SM. The coupling of three Higgses with the gauge boson can be summarized as

The other CP-odd component a_2 becomes the longitudinal component of the additional gauge boson coming from $U(1)_{L_\mu - L_\tau}$ gauge symmetry and does not contribute in the CP-odd scalar mass matrix, M^2_A. After diagonalizing the mass matrix shown by Eq. (16), we get the following masses:

$$M^2_A = -\frac{\mu v_{\phi_1}}{\sqrt{2}}\left(\frac{v_1}{v_2}+\frac{v_2}{v_1}+\frac{v_1 v_2}{v^2_{\phi_1}}\right), \quad M^2_{G^0} = 0, \quad M^2_a = 0. \quad (17)$$

The mass eigenbasis $(AG^0 a)$ and flavor eigenbasis $(A_1 A_2 a_1)$ can be related by the following matrix relation:

$$\begin{pmatrix} G^0 \\ A \\ a \end{pmatrix} = U \begin{pmatrix} A_1 \\ A_2 \\ a_1 \end{pmatrix}, \quad (18)$$

where

$$U = \frac{1}{\sqrt{\sec^2\beta + \left(\frac{v_2}{v_{\phi_1}}\right)^2}} \begin{pmatrix} \cos\beta\sqrt{\sec^2\beta + \left(\frac{v_2}{v_{\phi_1}}\right)^2} & \sin\beta\sqrt{\sec^2\beta + \left(\frac{v_2}{v_{\phi_1}}\right)^2} & 0 \\ -\tan\beta & 1 & \frac{v_2}{v_{\phi_1}} \\ -\frac{v_2}{v_{\phi_1}}\sin\beta & \frac{v_2}{v_{\phi_1}}\cos\beta & -\sec\beta \end{pmatrix}. \quad (19)$$

$$\begin{aligned} g_{h_1 VV} &= c_{\alpha_2} c_{\beta-\alpha_1} \\ g_{h_2 VV} &= c_{\alpha_3} s_{\beta-\alpha_1} - s_{\alpha_2} s_{\alpha_3} c_{\beta-\alpha_1} \\ g_{h_3 VV} &= -s_{\alpha_3} s_{\beta-\alpha_1} - s_{\alpha_2} c_{\alpha_3} c_{\beta-\alpha_1}. \end{aligned} \quad (21)$$

In the limit $\beta - \alpha_1 = \frac{\pi}{2}$, $\alpha_{2,3} \to 0$, we go back to the 2HDM misalignment limit and h_2 coincides with the SM Higgs. In our analysis, we are going to consider h_2 as the SM Higgs field and fix its mass at $M_{h_2} = 125.5$ GeV. We are going to summarize the scalar couplings to fermion which will be needed for studying the muon $(g-2)$. Therefore, the Lagrangian associated with the scalars and the fermions take the following form:

$$\begin{aligned} \mathcal{L}_{Yuk} = &-\sum_f \left(\lambda_u^{h_i}\frac{m_f}{v}\bar{f}f h_i - i\lambda_f^{A_j}\frac{m_f}{v}\bar{f}\gamma^5 f A_j\right) \\ &+ \left[\sqrt{2}V_{ud}H^+\bar{u}\left(y_u^{H^\pm}\frac{m_u}{v}P_L + y_d^{H^\pm}\frac{m_d}{v}P_R\right)d\right. \\ &\left. + y_l^{H^\pm}\frac{\sqrt{2}m_l}{v}H^+\bar{\nu}_L l_R + \text{H.c.}\right], \end{aligned} \quad (22)$$

where the coefficients y_f^ϕ are shown in Table IV and they become equal to 1 in the misalignment limit described before for the SM Higgs field h_2.

TABLE IV. Coefficients of the scalars with the fermions where the full Lagrangian is represented in Eq. (22). In the table, the indices i, j for the CP-even and CP-odd scalars vary as $i = 1, 2, 3$ and $j = 2, 3$.

Type	$\lambda_u^{h_i}$	$\lambda_d^{h_i}$	$\lambda_l^{h_i}$	$\lambda_u^{A_j}$	$\lambda_d^{A_j}$	$\lambda_l^{A_j}$	$\lambda_u^{H^\pm}$	$\lambda_d^{H^\pm}$	$\lambda_l^{H^\pm}$
I	$\frac{R_{i2}}{\sin\beta}$	$\frac{R_{i2}}{\sin\beta}$	$\frac{R_{i2}}{\sin\beta}$	$\frac{U_{i2}}{\sin\beta}$	$-\frac{U_{i2}}{\sin\beta}$	$-\frac{U_{i2}}{\sin\beta}$	$\cot\beta$	$-\cot\beta$	$-\cot\beta$
II	$\frac{R_{i2}}{\sin\beta}$	$\frac{R_{i1}}{\cos\beta}$	$\frac{R_{i1}}{\cos\beta}$	$\frac{U_{i2}}{\sin\beta}$	$-\frac{U_{i1}}{\cos\beta}$	$-\frac{U_{i1}}{\cos\beta}$	$\cot\beta$	$\tan\beta$	$\tan\beta$
X	$\frac{R_{i2}}{\sin\beta}$	$\frac{R_{i2}}{\sin\beta}$	$\frac{R_{i1}}{\cos\beta}$	$\frac{U_{i2}}{\sin\beta}$	$-\frac{U_{i2}}{\sin\beta}$	$-\frac{U_{i1}}{\cos\beta}$	$\cot\beta$	$-\cot\beta$	$\tan\beta$
Y	$\frac{R_{i2}}{\sin\beta}$	$\frac{R_{i1}}{\cos\beta}$	$\frac{R_{i2}}{\sin\beta}$	$\frac{U_{i2}}{\sin\beta}$	$-\frac{U_{i1}}{\cos\beta}$	$-\frac{U_{i2}}{\sin\beta}$	$\cot\beta$	$\tan\beta$	$-\cot\beta$

III. NEUTRINO MASS

After the symmetry breaking, the Lagrangian as shown in Eq. (5) gives us the neutrino mass matrix in the basis $(\nu_L^c N_f)$ as follows:

$$\mathcal{L}_{\text{neutrino}} = \begin{pmatrix} \bar{\nu}_L & \bar{N}_f^c \end{pmatrix} \begin{pmatrix} 0 & M_D^T \\ M_D & M_R \end{pmatrix} \begin{pmatrix} \nu_L^c \\ N_f \end{pmatrix} + \text{H.c.}, \tag{23}$$

where the Dirac mass matrix (M_D) and the Majorana mass matrix (M_R) take the following form:

$$M_D = \begin{pmatrix} \frac{y_{ee}v_2}{\sqrt{2}} & 0 & 0 \\ 0 & \frac{y_{\mu\mu}v_2}{\sqrt{2}} & 0 \\ 0 & 0 & \frac{y_{\tau\tau}v_2}{\sqrt{2}} \end{pmatrix},$$

$$M_R = \frac{v_{\phi_1}}{\sqrt{2}M_{\text{pl}}} \begin{pmatrix} \lambda_{ee}^N M_{\text{pl}} & \frac{\lambda_{e\mu}v_{\phi_2}}{\sqrt{2}} & \frac{\lambda_{e\tau}v_{\phi_2}}{\sqrt{2}} \\ \frac{\lambda_{e\mu}v_{\phi_2}}{\sqrt{2}} & 0 & \lambda_{\mu\tau}^N M_{\text{pl}} e^{i\theta} \\ \frac{\lambda_{e\tau}v_{\phi_2}}{\sqrt{2}} & \lambda_{\mu\tau}^N M_{\text{pl}} e^{i\theta} & 0 \end{pmatrix}. \tag{24}$$

Once we diagonalize Eq. (23) in the seesaw limit, i.e., $M_D \ll M_R$, then we get light and heavy neutrino mass matrices as follows:

$$m_\nu = -M_D^T M_R^{-1} M_D, \qquad M_N = M_R. \tag{25}$$

Furthermore, upon the diagonalization of the m_ν we get three masses for the active neutrinos ($m_d^i, i = 1, 2, 3$) and diagonalization matrix referred to as the Pontecorvo–Maki–Nakagawa–Sakata (PMNS) matrix [49], $U_{\text{PMNS}}(\theta_{12}, \theta_{13}, \theta_{23})$, which are related as follows:

$$m_d = U_{\text{PMNS}}^T(\theta_{12}, \theta_{13}, \theta_{23}) m_\nu U_{\text{PMNS}}(\theta_{12}, \theta_{13}, \theta_{23}), \tag{26}$$

where $\theta_{ij}(i, j = 1, 2, 3)$ are the oscillation angles and the PMNS matrix takes the following form:

$$U_{\text{PMNS}} = \begin{pmatrix} c_{12}c_{13} & s_{12}c_{13} & s_{13}e^{-i\delta_{CP}} \\ -s_{12}c_{23} - c_{12}s_{23}s_{13}e^{i\delta_{CP}} & c_{12}c_{23} - s_{12}s_{23}s_{13}e^{i\delta_{CP}} & s_{23}c_{13} \\ s_{12}s_{23} - c_{12}c_{23}s_{13}e^{i\delta_{CP}} & -c_{12}s_{23} - s_{12}c_{23}s_{13}e^{i\delta_{CP}} & c_{23}c_{13} \end{pmatrix}, \tag{27}$$

where $c_{ij} = \cos\theta_{ij}$ and $s_{ij} = \sin\theta_{ij}$. The Dirac CP phase δ_{CP} can be determined using the Jarlskog invariant [50] as shown below:

$$\begin{aligned} J_{CP} &= \text{Im}[U_{\text{PMNS}}(\alpha, i) U_{\text{PMNS}}^*(\alpha, j) U_{\text{PMNS}}^*(\beta, i) U_{\text{PMNS}}(\beta, j)] \\ &= J_{CP}^{\max} \sin\delta_{CP} = c_{12}s_{12}c_{23}s_{23}c_{13}^2 s_{13} \sin\delta_{CP}. \end{aligned} \tag{28}$$

Finally, the matrix M_N represents the heavy neutrino mass matrix. It is worth pointing out that, due to the additional Abelian gauge symmetry, we have just enough free parameters to accommodate values for the oscillation parameters in the correct ballpark of values favored by the different oscillation experiments. To achieve such a result, however, all three right-handed neutrinos should participate to the seesaw mechanism. In other words, we cannot accommodate, in our setup, sterile neutrino DM by decoupling one of the right-handed neutrinos. This is an additional motivation, besides the interest on its own, for the introduction of axion DM. We also remark that the PQ controls the configuration of the Yukawa couplings of the Higgs doublets to the SM fermions. In the present work, we have considered lepton-specific (type-X) and type-II 2HDM. Let us finally move to neutrino masses. If we consider Universal Yukawa couplings for the Dirac and Majorana mass terms, then we can write them down as

$$M_D = \frac{y_{ii} v_2}{\sqrt{2}} (i = e, \mu, \tau) \text{ and } M_N = \frac{\lambda_{ij} v_{\phi_2} v_{\phi_1}}{2 M_{\rm pl}} (i, j = e, \mu, \tau). \tag{29}$$

In writing the (1,1) and (2,3) elements of the right-handed neutrino mass matrix [as shown in Eq. (24)] in the above format, we have considered $\lambda^N_{ee(\mu\tau)} = \frac{\lambda_{ee(\mu\tau)} v_{\phi_2}}{\sqrt{2} M_{\rm pl}}$. Therefore, the light neutrino mass matrix will take the form

$$\begin{aligned} m_\nu &= \frac{y_{ii}^2 v^2}{2 M_N} \left(\frac{\tan^2\beta}{1 + \tan^2\beta} \right) \\ &= \frac{y_{ii}^2 v^2 g' M_{\rm pl}}{\lambda_{ij} M_{Z'} v_{\phi_1}} \left(\frac{\tan^2\beta}{1 + \tan^2\beta} \right). \end{aligned} \tag{30}$$

Neutrino data from different measurements have put severe constraints on the mixing angles of the PMNS matrix and the mass square differences. The current bound on the mixing angles for normal ordering in the 3σ range is given by [4]

$$\begin{aligned} &\theta^0_{12} \to (31.31 \to 35.74), \qquad \theta^0_{13} \to (8.19 \to 8.89), \\ &\theta^0_{23} \to (39.60 \to 51.90), \end{aligned} \tag{31}$$

and the mass square differences as

$$\begin{aligned} \Delta m^2_{21} &\to (6.82 \to 8.03) \times 10^{-5}\ \text{eV}^2, \\ \Delta m^2_{31} &\to (2.428 \to 2.597) \times 10^{-3}\ \text{eV}^2. \end{aligned} \tag{32}$$

The ranges for the inverted ordering are also similar but Δm^2_{31} is with a negative sign. For the present structure of the neutrino mass ordering, one of the authors has already studied the neutrino mass and obtained the correct values of the oscillation parameters and showed that inverted mass ordering is not possible for this kind of mass matrix structure [51]. In the present work, we assume that the correct ranges of oscillation parameters can be achieved and instead study the range of the parameters which will give the feasible values for the Dirac and Majorana mass matrix; namely, if the associated Yukawa coupling for the Dirac mass term can be made larger than the electron Yukawa coupling and the Majorana mass terms above the keV range. This is necessary to check because the Planck suppresses some of the elements in the Majorana mass matrix mass term.

In the left and right parts of the upper panel of Fig. 1, we have shown scatter plots in the $v_{\phi_2} - v_{\phi_1}$ plane. The color variation in the left one is for the Dirac Yukawa coupling associated with the neutrinos and the right part is for the right-handed neutrino mass. Both of the plots are for the type-II 2HDM model. The lower panel represents the same plots but for the type-X 2HDM model. In generating the plots, we have considered the order of the neutrino mass $m_\nu = 10^{-11}$ GeV [as shown in Eq. (30)] and the Yukawa couplings for the right-handed neutrino mass matrix [shown by Eq. (29)] as $\lambda_{ij} = 1$ $(i, j = e, \mu, \tau)$. It is worth mentioning that all of the points in the plots can give us the correct value of muon $g-2$, the total amount of DM by suitably choosing the initial angle, and also contributing to the oblique parameters S, T, U which will be addressed in the next sections. In the left part of the upper panel, we can see that v_{ϕ_2} cannot be larger than 210 GeV and v_{ϕ_1} can take the values up to maximal varied range 10^{16} GeV. In the figure, we can see that for a fixed value v_{ϕ_1} if we increase the v_{ϕ_2} values then the Yukawa coupling y_{ee} starts increasing as depicted by the color variation. The variation in y_{ee} is not huge because v_{ϕ_2} does not vary in a large range for the type-II 2HDM case. On the other hand, if we move towards the increment of v_{ϕ_1} direction then we observe a large variation in y_{ee} because of the large varied range in v_{ϕ_1}. In the right part of the upper panel, we can see the color variation in right-handed neutrino mass. The right-handed neutrino masses depends on the VEVs $v_{\phi_{1,2}}$ as $M_N \propto v_{\phi_1} v_{\phi_2}$, therefore we see an anticorrelation between v_{ϕ_1} and v_{ϕ_2} if we take a fixed value of right-handed neutrino mass. Moreover, we see an increment in M_N as we move in any incremental direction of the VEVs $v_{\phi_{1,2}}$. From both parts of the figure, we can see that the right-handed neutrino mass can go to a maximum value of 1 GeV and the associated Dirac Yukawa coupling reaches at most 10^{-8}. Therefore, for the type-II case, we cannot achieve y_{ee} up to the value of the Yukawa coupling needed for the electron mass in SM. On the other hand, in the lower panel, we have shown the same thing but for large values of v_{ϕ_2} as well; this helps us in getting the y_{ee} as large as electron Yukawa coupling and the right-handed neutrino mass as large as 1 TeV. As we will see later for the type-X 2HDM, muon $g-2$ can also be achieved only by the Higgs sector which helps us to lower the gauge coupling g' and, hence, obtain the increased value of the VEV $v_{\phi_2} = \frac{M_{Z'}}{g'}$. Finally, low-mass right-handed neutrinos will be constrained by many experiments and will also be explored in the future by a number of experiments. A detailed discussion of the low mass right-handed neutrino detection prospects can be found in [52]. Moreover, as shown in Ref. [52], right-handed neutrino mass below 0.7 GeV will impact the Big Bang nucleosynthesis (BBN) bound [53–55]. This problem can be overthrown in the present context by choosing the appropriate values of $\lambda^N_{ee}, \lambda^N_{\mu\tau}$ (compatible with the neutrino oscillation data as shown in [51]) parameters in the right-handed neutrino mass matrix [see Eq. (24)] which makes the right-handed neutrino masses higher and can evade the BBN bound. For a precise statement in this context, we require full-fledged study and left this to pursue in the future. The baryogenesis process concerning the MeV scale right-handed neutrino mass within the type-I seesaw mechanism has been studied in Ref. [56] albeit the right-handed neutrino decay needed before BBN.

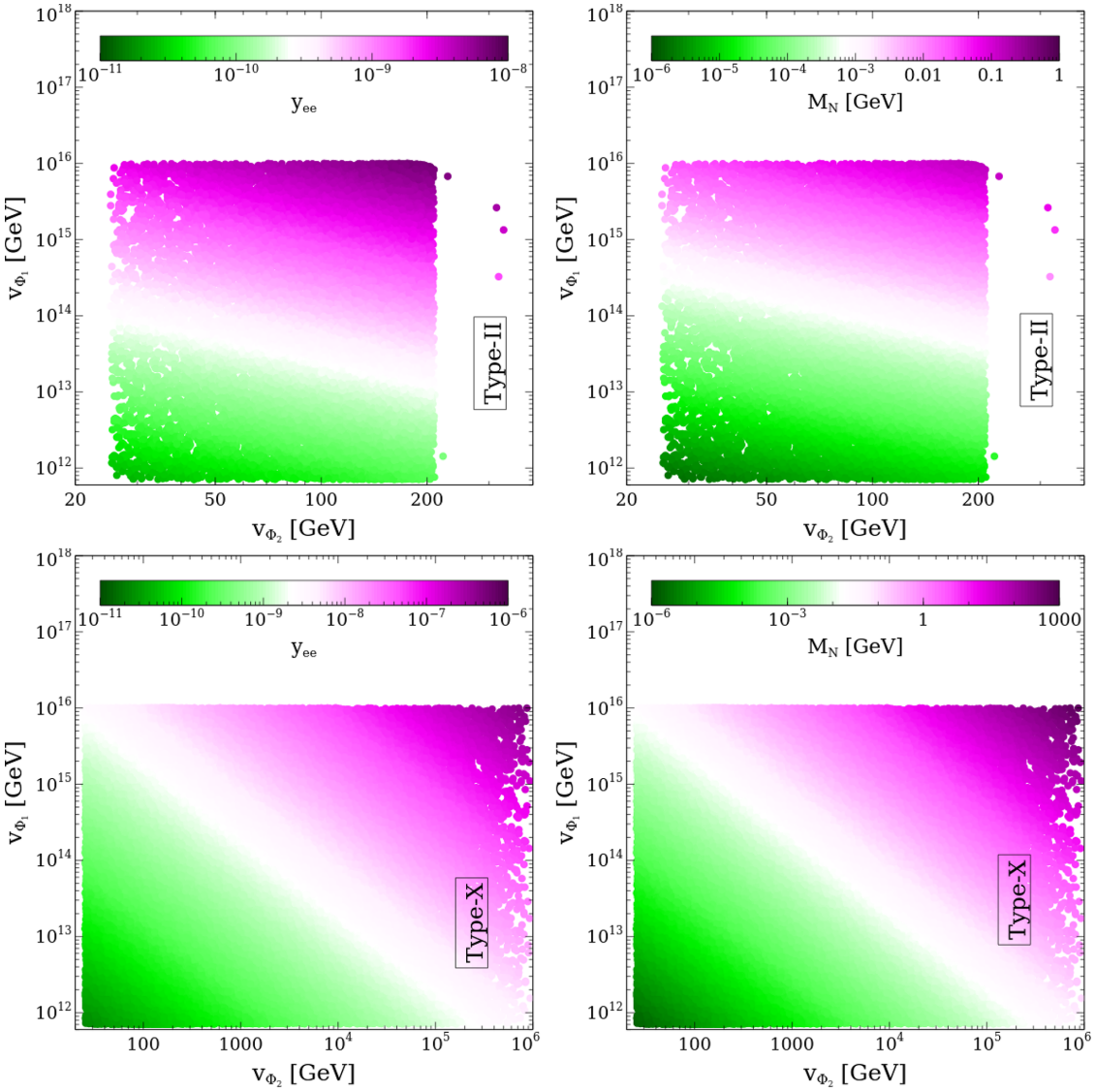

FIG. 1. Scatter plots in $v_{\phi_2} - v_{\phi_1}$ plane where in the left panel (LP) color variation corresponds to the Dirac Yukawa coupling for the neutrinos and right panel (RP) shows the color variation for the right-handed neutrino mass. The upper panel and lower panel correspond to the type-II and type-X 2HDM models.

In Table V, we have shown benchmark points after satisfying the neutrino oscillation data as shown in Eqs. (31) and (32). In the table, $M_{Dii} = \frac{y_{ii}v}{\sqrt{2}} (i = e, \mu, \tau)$ and M_{Rij} is the (i, j)th element of the right-handed neutrino mass matrix as shown in Eq. (24). As can be seen from the table, we can have a right-handed neutrino mass $\mathcal{O}(10)$ GeV and Dirac mass matrix around $\mathcal{O}(10^{-5})$ GeV and we can satisfy the neutrino oscillation data. As an estimate, we can see from Fig. 1 that right-handed neutrino mass $\mathcal{O}(1)$ GeV can be obtained for $v_{\phi_1} > 10^{15}$ GeV for type-II 2HDM and for type-X there is no stricter bound on v_{ϕ_1} because we can choose any values of v_{ϕ_2}. Therefore, the present model for the type-II 2HDM case demands higher values of the Peccei-Quinn scale if we want to explain $(g-2)_\mu$ in conjunction with the other phenomenologies. It is worth pointing out that the bound on v_{ϕ_1} can be alleviated for type-II 2HDM if we explain the other phenomenologies except for the muon $(g-2)$ anomaly. In the future, we plan to explore the more concrete bound on the Peccei-Quinn scale, which we expect to be around $v_{\phi_1} > 10^{15}$ GeV, from the neutrino oscillation and low-scale flavor physics data.

IV. AXION DM

In this work, we consider that the singlet scalar ϕ_1 takes spontaneous VEV (v_{ϕ_1}) which is around or above the inflation scale. This high VEV ensures that our axion field would be invisible to the visible sector due to its suppressed coupling impacted by the very high VEV. This also exhibits

TABLE V. Benchmark points after satisfying the neutrino oscillation data.

Parameters	BP1	BP2	BP3	BP4	BP5
M_{D11} [GeV]	1.37302×10^{-5}	3.97752×10^{-5}	5.20121×10^{-5}	4.92606×10^{-5}	3.74946×10^{-5}
M_{D22} [GeV]	3.057×10^{-5}	5.85732×10^{-5}	2.07667×10^{-5}	8.96679×10^{-5}	3.71355×10^{-5}
M_{D33} [GeV]	3.32727×10^{-5}	6.36453×10^{-5}	2.61519×10^{-5}	5.53581×10^{-5}	1.51743×10^{-5}
M_{R11} [GeV]	2.70458	24.9567	39.2377	38.6315	20.2238
M_{R23} [GeV]	15.4077	58.6951	7.57553	78.6556	8.10739
M_{R12} [GeV]	5.20407	28.0349	9.6568	53.6334	14.9338
M_{R13} [GeV]	4.7754	36.708	14.1577	40.0791	5.23469
θ[rad]	3.10937	3.17792	3.16356	3.17936	3.16513
$\frac{\Delta m^2_{21}}{10^{-5}\ \mathrm{eV}^2}$	7.82389	6.94169	7.29951	7.34332	6.84982
$\frac{\Delta m^2_{31}}{10^{-3}\ \mathrm{eV}^2}$	2.4923	2.49091	2.57468	2.47229	2.46313
$\theta_{12}[^0]$	32.6683	34.4914	31.6346	33.65	33.066
$\theta_{23}[^0]$	40.2752	50.1825	49.231	50.2849	40.721
$\theta_{13}[^0]$	8.46868	8.54961	8.66937	8.67221	8.61547
$\delta_{CP}[^0]$	248.527	327.199	159.552	144.312	153.267
$\sum m_\nu$[eV]	0.155288	0.145748	0.175355	0.144533	0.169207

that the associated neutral *CP*-even Higgs would also be very heavy and can be approximated as $M^2_{\phi_1} \simeq \lambda_{\phi_1} v^2_{\phi_1}$. This mass eigenstate has the mixing term with the SM Higgs and will contribute to Higgs mass radiatively as

$$M^2_{h_2} = M^2_{h_2,\mathrm{tree}} + \lambda_{H_i\phi_1}\left[\Lambda^2_{\mathrm{UV}} + M^2_{\phi_1}\log\left(\frac{M^2_{\phi_1}}{\Lambda^2_{\mathrm{UV}}}\right)\right]. \tag{33}$$

Here $M^2_{\phi_1}$ is a physical parameter and cannot be removed by introducing the counterterms. As discussed in [57], if we go in the limit $\lambda_{H_i\phi_1} \to 0\,(i = 1, 2)$, then we go in the regime of the enhanced Poincaré symmetry and we can protect the light SM Higgs mass. The bound on the quartic couplings which relate the SM Higgs and ϕ_1 is the following:

$$\lambda_{H_i\phi_1} \leq \mathcal{O}\left(\frac{M_h}{M_{\phi_1}}\right), \qquad (i = 1, 2). \tag{34}$$

Therefore, in this work, we consider $\lambda_{H_i\phi_1} \to 0$ and the field ϕ_1 couple to the SM sector very feebly and do not alter our phenomenology presented in this work. Therefore, the neutral Higgs mass matrix as given in Eq. (10) effectively reduces to 3×3 matrices which can be diagonalized by the orthogonal matrix R shown in Eq. (12).

A. PQ symmetry

As discussed before in the present work, we can introduce the $U(1)_{\mathrm{PQ}}$ symmetry with the charge assignment shown in Table III and when it breaks spontaneously we can have a massless axion field. As pointed out in Refs. [31–35], the global Abelian symmetry is not a good symmetry up to the Planck scale, so it is unpleasing to introduce a global $U(1)$ symmetry barely in the SM because it will not be valid up to the Planck scale. This situation can be evaded if PQ symmetry appears accidentally and can be achieved by introducing the discrete symmetries as studied in [24–28]. Therefore, we can always decide on the discrete symmetries which ensures the accidental appearance of the PQ symmetry as well as does not alter our phenomenology. This way we can solve the potential problem regarding the validity of global PQ symmetry up to the Planck scale. As studied in Ref. [29], the additional discrete symmetries might arise as residual symmetries when additional gauge symmetries spontaneously break, remaining unaffected from the gravity-induced breaking. Therefore, to have a suitable discrete symmetries as residual symmetries, we need to assign the gauge charges to the particle content accordingly under the new gauge symmetry as studied in Ref. [29]. In this work, the Higgs doublets and fermions are charged under the $U(1)_{\mathrm{PQ}}$ symmetry which makes the present model like DFSZ kind [39,40] axion model in contrary to the Kim–Shifman–Vainshtein–Zakharov (KSVZ) type model [58–60], where one needs to introduce extra exotic quarks in order to generate axion-gluon coupling. In the present work, we consider singlet-dominated pseudoscalar "a" as the axion field with axion decay constant $v_a = \sqrt{v^2_{\phi_1} + \frac{v^2_1 v^2_2}{v^2}} \simeq v_{\phi_1}$, for $v_{\phi_1} \gg v, v_{1,2}$. By using the diagonalization matrix as shown in Eq. (18), we can write down the $A_{1,2}$ in terms of the axion field like $\frac{A_1}{v_1} \to X_{H_1}\frac{a}{v_a}$, $\frac{A_2}{v_2} \to X_{H_2}\frac{a}{v_a}$, and $\frac{a_1}{v_{\phi_1}} \to X_{\phi_1}\frac{a}{v_a}$, where X_F is the PQ charge of the field $F\ (= H_{1,2}, \phi_1)$. We can write down the mass term for the quarks and leptons consist of the axion field as

$$\begin{aligned}\mathcal{L}_{a-\mathrm{mass}} \supset & -m_u \bar{u}_L u_R e^{-iX_{H_2}\frac{a}{v_a}} - m_d \bar{d}_L d_R e^{-iX_{H_m}\frac{a}{v_a}} \\ & - m_l \bar{l}_L l_R e^{-iX_{H_n}\frac{a}{v_a}} + \mathrm{H.c.}\end{aligned} \tag{35}$$

We can now get rid of the phase factor terms consisting of the axion field by redefining the fields as

$$u \to e^{i\gamma_5 X_{H_2}\frac{a}{2v_a}}u, \quad d \to e^{-i\gamma_5 X_{H_m}\frac{a}{2v_a}}d, \quad l \to e^{-i\gamma_5 X_{H_n}\frac{a}{2v_a}}l. \quad (36)$$

This way of redefining the fields will induce the anomaly associated with the QCD and electromagnetic (EM) fields. These anomaly terms can be written in terms of the QCD and EM fields as

$$\mathcal{L}_{\text{anomaly}} = \frac{\alpha_s}{8\pi}\frac{a}{F_a}G\tilde{G} + \frac{\alpha_{\text{EM}}}{8\pi}\frac{E}{N}\frac{a}{F_a}F\tilde{F}, \quad (37)$$

where $F_a = \frac{v_a}{|2N|}$. N and E are, respectively, the anomaly factors depend on the QCD and EM charges coming from the $SU(3)_c \times SU(3)_c \times U(1)_{\text{PQ}}$ and $U(1)_{\text{EM}} \times U(1)_{\text{EM}} \times U(1)_{\text{PQ}}$ anomaly terms. The EM sector anomaly term E and strong sector anomaly term N can be expressed in terms of the PQ charges as [46]

$$N = 3\left(-\frac{1}{2}X_{H_2} + \frac{1}{2}X_{H_m}\right),$$
$$E = 3\left(-3\left(\frac{2}{3}\right)^2 X_{H_2} + 3\left(-\frac{1}{3}\right)^2 X_{H_m} + (-1)^2 X_{H_n}\right). \quad (38)$$

The values of N and E will depend on the m, n values which represent the different kind of 2HDM as shown in Table VI.

The PQ charge of the SM and the BSM particles are given in Table III. As can be seen from Eq. (6), the PQ symmetry breaks when the field ϕ_1 gets VEV and the axion potential is generated at the QCD phase transition by the instanton effects. Therefore, the periodic potential for the dynamical field axion can be expressed as [46]

$$V_{\text{QCD}}(a) = M_a^2 F_a^2(1 - \cos[\theta_a + \bar{\theta}]), \quad (39)$$

where F_a is axion decay constant, $\theta_a = \frac{a}{F_a}$, and M_a is the axion mass given by [46]

$$M_a^2 = \frac{m_u m_d}{(m_u + m_d)^2}\frac{f_\pi^2 m_\pi^2}{F_a^2} \simeq 5.7\left(\frac{10^{12}\ \text{GeV}}{F_a}\right)\ \mu\text{eV}, \quad (40)$$

TABLE VI. N and E values for different types of 2HDM models.

Type	N	E	E/N
I	0	0	⋯
II	−3/2	−4	8/3
X	0	−3	⋯
Y	−3/2	−1	2/3

where $m_{u,d}$ are the quark masses, $f_\pi = 130$ MeV is the pion decay constant, and $m_\pi = 139.57$ MeV is the pion mass. In the axion potential, we can define a new field after redefining it as $\overline{\theta_a} = \theta_a + \bar{\theta}$. In Eq. (39), we have shown the axion potential which will appear when the axion has coupling with the gluons, so in the present model type-II and type-Y 2HDM fall into this category. Therefore, we can solve the strong CP problem for these two variants of the 2HDM model. Moreover, the axion appears from type-II and type-Y 2HDM and can also be a good DM candidate which can be produced by the misalignment mechanism [61]. On the other hand, type-I and type-X 2HDM models have no coupling between axion and gluon fields so the axion does not have potential as shown in Eq. (39), therefore they cannot solve the strong CP problem. But they can be a good DM candidate and produced by the misalignment mechanism [62]. Moreover, their mass can be produced at the Planck scale by the PQ violating terms [60] and we can produce them by the usual misalignment mechanism. In this work, we have considered DM production only for the QCD-type axion field and can also be estimated for the axionlike particle by following Ref. [62].

B. Axion density

The axion can be a very good cold DM candidate and is produced in the early Universe by the misalignment mechanism [61]. The amount of axion density depends on the axion decay constant (F_a) and the initial misalignment angle θ_i and quantitatively can be expressed as [61]

$$\Omega_a h^2 = 0.12\theta_i^2\left(\frac{F_a}{10^{12}\ \text{GeV}}\right)^{1.19}. \quad (41)$$

If we consider the PQ symmetry breaking before the inflation scale then θ_i can take any arbitrary value and, if it breaks after inflation, we need to take the average values of θ_i over the different patches and take the value [63]

$$\theta_i \simeq \sqrt{\langle\theta_i^2\rangle} \sim 2.15. \quad (42)$$

In this work, we consider the PQ symmetry breaking before the inflation so we can ignore the contribution in the axion density from the cosmological defects; otherwise, one needs to take into account the axion density coming from the domain wall, strings [64–67]. Moreover, in this work, we have not considered axion production in the early Universe via thermal scattering because it will be subdominant for the axion decay constant F_a considered here [68]. This mode of axion production can also contribute to the relativistic degree of freedom (ΔN_{eff}) of the Universe. This bound is weak in our case because, as found in Ref. [68], the recent bound on ΔN_{eff} from the Planck data [9] requires $F_a > 10^7$ GeV, which is weaker

than the supernovae bound of $F_a > 2 \times 10^8$ GeV [41] considered in this work.

C. Isocurvature bounds

As studied in Refs. [69,70], if the PQ breaking happens during or before the inflation then the massless axion can have quantum fluctuations which will contribute to the total energy density of the axion. The quantum fluctuation of the axion field is given by

$$\delta a = \frac{H_{\rm inf}}{2\pi}, \tag{43}$$

where $\delta a = F_a \delta\theta_i$ and $H_{\rm inf}$ is the Hubble parameter during inflation.

The axion fluctuation can generate the isocurvature perturbation, $S_{\rm DM}$, which is defined as [69]

$$S_{\rm DM} = \Omega_a^{\rm frac} h^2 \frac{\delta\rho_a}{\rho_a}, \tag{44}$$

where $\Omega^{\rm frac} h^2 = \frac{\Omega_a h^2}{\Omega_{\rm DM} h^2}$ is the fraction of the DM contained by the axion field. The CMB data [71,72] has put a tight bound on the isocurvature perturbation which gives the bound in the inflation scale as [70]

$$H_{\rm inf} \leq 2.4 \times 10^7 \text{ GeV} \left(\frac{F_a}{10^{12} \text{ GeV}}\right)^{0.405}. \tag{45}$$

The isocurvature perturbation also contributes to the axion density and changes Eq. (41) as follows:

$$\Omega_a h^2 = 0.18 \left[\theta_i^2 + \left(\frac{H_{\rm inf}}{2\pi F_a}\right)^2\right] \left(\frac{F_a}{10^{12} \text{ GeV}}\right)^{1.18}. \tag{46}$$

In Fig. 2, we have shown scatter plots in the $F_a - H_{\rm inf}$ plane where the color variation in both panels is represented by θ_i and $\frac{\Omega_a^{\rm isoc} h^2}{\Omega_{\rm DM} h^2} \times 100[\%]$. In generating the plots, we have varied the parameters in the following range:

$$\begin{aligned} 10^{-3} \leq \theta_i \leq 1 \\ 10^5 \text{ GeV} \leq H_{\rm inf} \leq 10^7 \text{ GeV} \end{aligned} \tag{47}$$

and the axion DM relic density has been demanded in the 3σ range put by Planck [9,73], i.e., $0.1172 \leq \Omega_{\rm DM} h^2 \leq 0.1226$. In the left panel (LP), we look at the upper line which begins at $H_{\rm inf} = 3 \times 10^6$ GeV then it exhibits that the DM relic density is independent of θ_i for the range in which it has been varied. The line also implies that if we take the inflation scale above this line, there will be an overproduction of DM. Below this line or lower values of $H_{\rm inf}$ we can see that DM production depends on θ_i and the axion produced mainly by the misalignment mechanism. We can see from the LP that if we increase the F_a value then we need lower values of θ_i to satisfy the DM relic density in the 3σ range. On the other hand, in the right panel (RP), the color bar corresponds to the contribution to the axion density from the isocurvature perturbation. We can see if we take $H_{\rm inf} > 3 \times 10^6$ GeV then the DM is overproduced from the isocurvature contribution and as we go to lower values of $H_{\rm inf}$ then we get lower contribution in the axion density from axion fluctuation and more contribution starts coming from the misalignment mechanism.

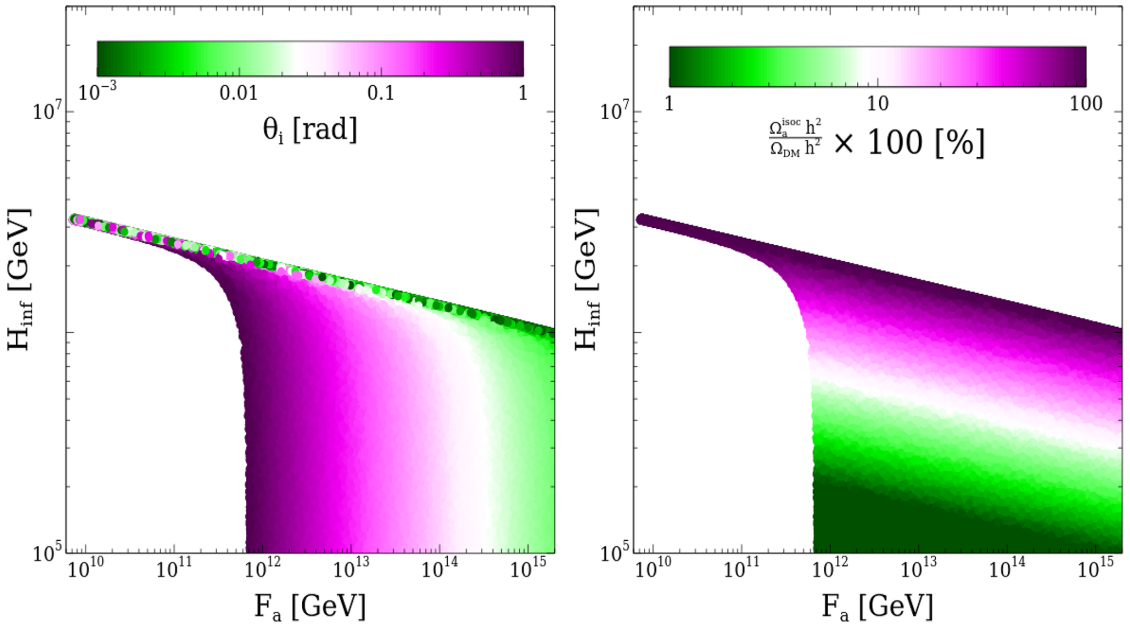

FIG. 2. Scatter plots in the $F_A - H_{\rm inf}$ plane after satisfying the axion density in the 3σ range of dark matter relic density put by Planck. The color bar corresponds to different values of θ_i and percentage of axion density from isocurvature fluctuation in the LP and RP, respectively.

D. Axion DM searches

There have been several attempts to detect the axion type DM at the haloscope experiments and also proposals for future exploration in the context of the DFSZ and KSVZ types of axion model. A detailed discussion on the detection prospects by using different techniques has been exhibited in Ref. [46]. In particular, the axion dark matter experiment (ADMX) has already probed the axion mass range 2.7–4.2 μeV, using haloscope for axion dark matter, which represents the total amount of DM for $\mathcal{O}(1)$ misalignment angle [74–76]. There is also an attempt to explore the higher mass range, for example CAPP-8TB [77], which aims to probe the axion mass range 6.62–7.04 μeV with the follow-up proposal like CAPP-12TB and CAPP-25T [78]. Another dielectric haloscope experiment MADMAX [79] can probe the axion mass range 50–100 μeV. On the other hand, probing the lower mass range of axion DM needs a larger haloscope which is more challenging. The KLASH experiment [80] aims to explore the axion mass range 0.3–1 μeV. There is also an attempt to explore the axion mass range below 10^{-8} eV using different techniques. ABRACADABRA [81] is one such attempt which can detect oscillating magnetic flux through the center of the toroid produced by the axion and posed the possibility to detect the axion DM mass range below 10^{-8} eV. They have already explored the mass range $(3.1\text{–}83.0) \times 10^{-10}$ eV from one-month data collection with ABRACADABRA-10 cm.

V. MUON $(g-2)$

In this section, we are going to address the muon $(g-2)$ anomaly which SM cannot explain but the present model has the potential to explain it. The SM contribution to $(g-2)_\mu$ has been measured very precisely after taking into account all the contributions; namely, quantum electrodynamics (QED), hadronic vacuum polarization, hadronic light by light, and electroweak processes. Based on the aforementioned contributions, SM predicts the muon $(g-2)$ contribution as $a_\mu(\mathrm{SM}) = 116591810(43) \times 10^{-11}$ (0.37 ppm) [5]. Moreover, with the advancement of experimental techniques, there is also an attempt to measure the muon $(g-2)$ experimentally. The main contributors in the measurement of muon $(g-2)$ experimentally include CERN [82–85], BNL E821 [86] at Brookhaven, and the recent measurement by the FNAL [19]. BNL and FNAL have followed the same techniques to measure the muon spin precision in the magnetic field and agree with each other. The world average value in the present time from different experiments is $a_\mu(\mathrm{exp}) = 116592061(41) \times 10^{-11}$ (0.35 ppm). Therefore, the difference between the experimental and theoretical prediction from SM is [5,19]

$$\begin{aligned}\Delta a_\mu &= a_\mu(\mathrm{exp}) - a_\mu(\mathrm{SM}) \\ &= (251 \pm 59) \times 10^{-11}\end{aligned} \tag{48}$$

which implies a 4.2σ discrepancy between the experimental and theoretical values. It is worth mentioning here that the recent advancement in lattice computation measured the hadronic vacuum polarization which differs from the different experimental measurements of the hadronic vacuum polarization by 2.1σ [20]. Therefore, it reduces the significance of the discrepancy between the experiment and theory to 1.5σ [20]. Moreover, a new measurement by CMD-3 experiments for vacuum hadronic polarization (VHP) contribution to the theoretical prediction indicates that the theoretical and experimental values are closer than before with 2.4σ discrepancy [21]. This new finding also poses a conflict with the previous measurements of $e^+e^- \to \pi^+\pi^-$ by the same and different experiments [87–90]. In summary, new data are required to definitively assess that the measure of $(g-2)$ really represents a deviation with respect to the SM prediction. Having this in mind we take, anyway, the hypothesis, for this work, that new physics is responsible for the $g-2$ anomaly. In the scenario under scrutiny, there are two kinds of BSM contributions to the anomalous magnetic moment of the muon. The first come from the extended Higgs sector, see, e.g., [91–95], while the other comes from the additional gauge boson [51,96–99]. We will see that both contributions are important in order to explain the muon $(g-2)$. As we have explained before, we need a positive contribution from the BSM physics in order to address the $(g-2)_\mu$ anomaly. In the case of scalar sector contribution, we have one-loop and two-loop contributions. The one-loop contribution can be summarized as [100–104]

$$\Delta a_\mu^{1-\mathrm{loop}} = \frac{G_F m_\mu^2}{4\pi^2\sqrt{2}} \sum_j (y_\mu^j)^2 r_\mu^j f_j(r_\mu^j), \tag{49}$$

where $j = \{h_1, h_2, h_3, A, a, H^\pm\}$, G_F is Fermi constant, $r_\mu^j = \frac{m_\mu^2}{M_j^2}$ (m_μ is muon mass and M_j is the mediator scalar mass), and the function $f_j(r)$ has the following form:

$$\begin{aligned} f_{h_{1,2,3}}(r) &= \int_0^1 dx \frac{x^2(2-x)}{1-x+rx^2}, \\ f_{A,a}(r) &= \int_0^1 dx \frac{-x^3}{1-x+rx^2}, \\ f_{H^\pm}(r) &= \int_0^1 \frac{-x(1-x)}{1-(1-x)r}. \end{aligned} \tag{50}$$

The normalized Yukawa coupling is defined as $L_{jff} = y_\mu^j(\frac{m_f}{v}) j\bar{f}f$ and given in Table III. The contribution from the scalar sector comes from the diagrams mediated by $h_{2,3}, A, a$ and we have ignored the contribution from the SM like Higgs h_1 because we work in the misalignment limit $\beta - \alpha = \frac{\pi}{2}$ and its contribution is already taken in the standard computation of Δa_μ.

From the previous expressions of the one-loop contribution to Δa_μ, we can see that the contribution is proportional to the fourth power of the muon mass. It has been shown in [105–107] that the two-loop contribution which is proportional to the heavier fermions can contribute significantly compared to the one-loop contribution. The two-loop contribution comes from the Bar-Zee type diagram and contributes to the $(g-2)_\mu$ by the following amount [105–107]:

$$\Delta_\mu^{2-\text{loop}} = \frac{G_F m_\mu^2}{4\pi^2\sqrt{2}} \frac{\alpha_{\text{EM}}}{\pi} \sum_{j,f} N_f^c Q_f^2 y_\mu^j y_f^j r_f^j g_i(r_f^j), \quad (51)$$

where j is as defined earlier and $f = b$ quark, t quark, and N_f^c, y_f^j, Q_f represent the color degree of freedom, associated Yukawa coupling of fermion f with the scalar j, and electromagnetic charge of mediator fermion f. The function $g_i(x)$ can be expressed as

$$g_i(x) = \int_0^1 dx \frac{\mathcal{N}_i(x)}{x(1-x)-r} \log\frac{x(1-x)}{r}, \quad (52)$$

where $\mathcal{N}_{h_{1,2,3}} = 2x(1-x)-1$ and $\mathcal{N}_{A,a}(x) = 1$. As discussed before, in the two-loop contribution as well we have not taken into account the SM Higgs contribution.

Moreover, in the present work, we also have the one-loop contribution mediated by the $U(1)_{L_\mu - L_\tau}$ gauge boson and has the following contribution to the $(g-2)_\mu$ [108,109]:

$$\Delta a_\mu^{Z'} = \frac{g'^2}{8\pi^2} \int_0^1 dx \frac{2x(1-x)^2}{(1-x)^2 + rx}. \quad (53)$$

As evidenced in the next section, the interplay of the different kinds of contributions allows us to reproduce the $(g-2)$ anomaly in a relatively large parameter space.

VI. RESULTS: ALLOWED PARAMETER REGIONS IN DIFFERENT PLANES

We are now going to display allowed regions among the parameters by performing a scan over the ranges summarized below. Each parameter assignation has been subject to bounds from DM relic density, $(g-2)$ as well as the theoretical bounds mentioned in Sec. B. Only the model points passing all of these constraints have been retained. For what concerns the 2HDM configurations, we have just focused on the type-II and type-X scenarios. Notice that in the type-II scenario, we have imposed *a priori* the bound $M_{H^\pm} > 800$ GeV to comply automatically with the bounds on $b \to s\gamma$ [110]. Reference [110] also mentioned that, for $\tan\beta < 2$, the bound will change, so in our study we have considered $\tan\beta > 2.5$ throughout the paper. We will discuss in detail the scanning plots that will exhibit the correlations among the parameters and will deliver us a broader idea about the choice of the model parameters. Additionally, in the case of type-X 2HDM, we are about to see that the parameters are more relaxed but it does not provide us with the effective coupling between the axion and the gluons (see Sec. IV). Therefore, we choose to study the type-II (type-X) 2HDM scenario which serves our purpose of having axion DM. We have varied our model parameters in the following range:

$$\begin{aligned}
&2.5 \le \tan\beta \le 250, \qquad 65 \le M_{h_1}[\text{GeV}] \le 1500, \qquad 125 \le M_{h_3}[\text{GeV}] \le 1500,\\
&10^{11} \le v_{\phi_1}[\text{GeV}] \le 10^{16}, \qquad 10^{-6} \le g' \le 10^{-2}, \qquad 10^{-3} \le M_{Z'}[\text{GeV}] \le 1,\\
&800(80) \le M_{H^\pm}[\text{GeV}] \le 1500, \qquad 10^5 \le M_{\phi_1}\ \text{GeV} \le 10^6, \qquad \beta - \alpha_1 \simeq \frac{\pi}{2},\\
&10^{-4} \le \alpha_{2,3} \le 10^{-1}, \qquad 10^{-4} \le \lambda_1 \le 4\pi. \qquad (54)
\end{aligned}$$

We have considered h_2 as the SM Higgs and kept its mass fixed at $M_{h_2} = 125.5$ GeV. The mass for the CP-odd scalars A, a depends on the VEVs, quartic couplings $(\lambda_{1,2})$, scalar mass and mixing angles, and have been evaluated automatically during the scanning of the parameters. The parameter μ has been measured using the quartic coupling λ_1 and the other Higgs masses and mixing angles.

In Fig. 3, we have shown scatter plots in the $M_A - M_{h_1}$ and $\lambda_{12} - \lambda'_{12}$ planes after satisfying DM total relic density, muon $(g-2)$ and the perturbativity and bound from the below conditions on the quartic couplings. In the upper panel, we have shown the result for the type-X 2HDM model and in the lower panel we have shown it for type-II 2HDM. In scanning the parameters, we have used the usual misalignment mechanism in 2HDM and h_2 as the SM like Higgs with mass 125.5 GeV. Let us first discuss the upper panel and the lower panel will be followed thereafter. We see a sharp correlation between M_A and M_{h_1} because the scatter plot follows the $M_A = M_{h_1}$ line represented by the red line. In general, the quartic coupling λ_1 depends on the masses of the scalars and the $\tan\beta$ for $\alpha_{2,3} \sim 0$, so in the misalignment limit it can be expressed as

$$\lambda_1 \simeq \frac{1}{2v_1^2}[(M_{h_1}^2 - M_A^2)\sin^2\beta + \cos^2\beta M_{h_2}^2]. \quad (55)$$

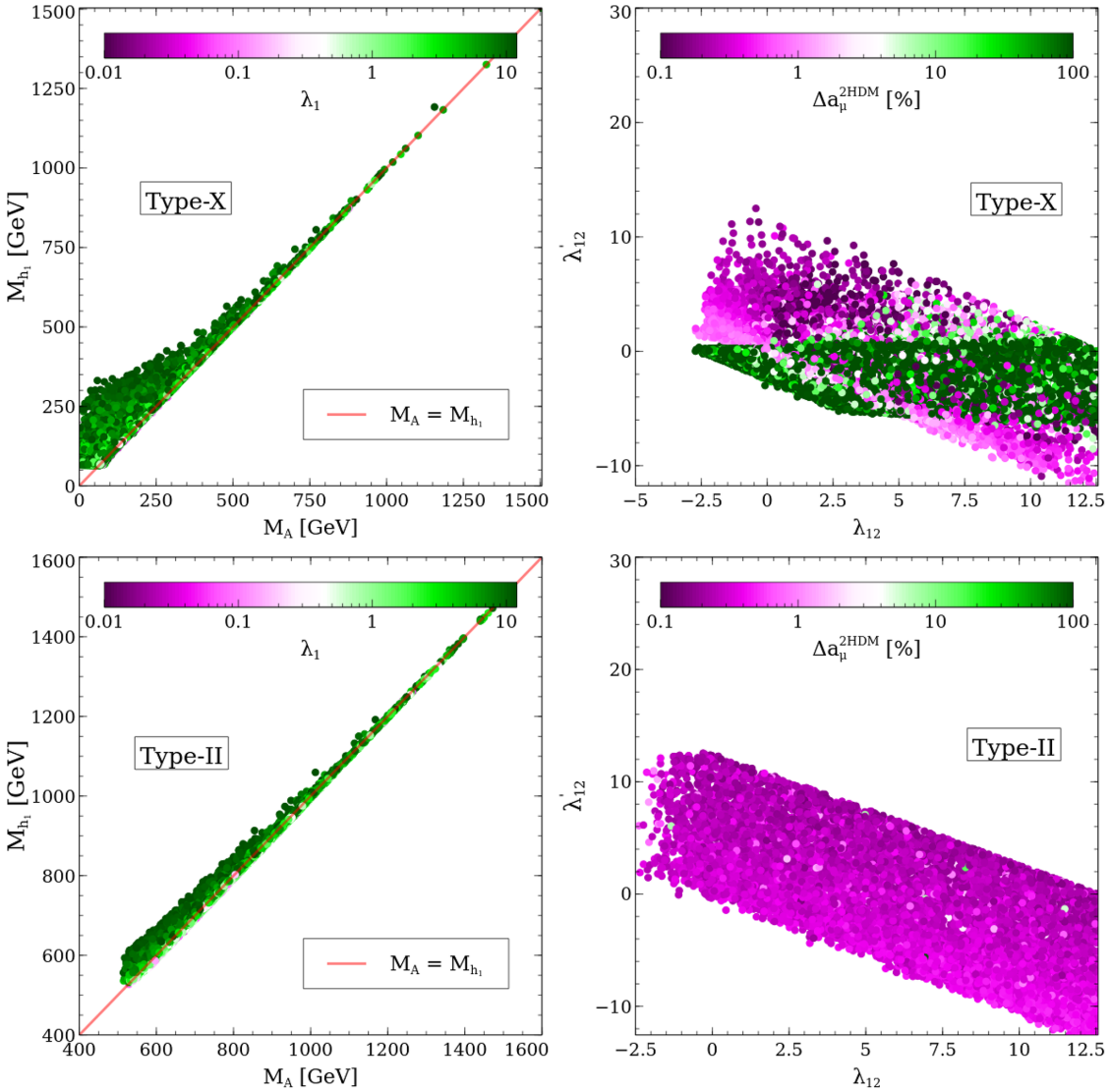

FIG. 3. Left panel: scatter plot in the $M_A - M_{h_1}$ plane after satisfying all the relevant bounds where the color bar corresponds to the different values of quartic coupling λ_1 associated with the Higgs doublet H_1. Right panel: scatter plot in the $\lambda_{12} - \lambda'_{12}$ plane and the color bar represents the contribution of the Higgs sector to muon $(g-2)$ in percentage.

For larger values of $\tan\beta$, we have $\cos\beta \ll 1$ and $\sin\beta \sim 1$, then the λ_1 will be smaller than 4π only when we have $M_A \sim M_{h_1}$, i.e, represented by the red diagonal line. In the other regime when we have $\sin\beta \ll 1$ and $\cos\beta \sim 1$, then we can go for $M_{h_1} > M_A$ because it is suppressed by $\sin\beta$ and at the same time $v_1 \sim v$, so the coupling additional suppression will happen due to the larger values of v_1 which is not possible for $\tan\beta \gg 1$. The points that are outside the $M_A \sim M_{h_1}$ line correspond to the larger values of λ_1. On the other hand, the points that are on the red line can take $\lambda_1 < 0.1$ because of the possibility of the exact cancellation among the masses. In the RP, we have shown the scatter plot in the $\lambda_{12} - \lambda'_{12}$ plane. We see that λ_{12} and λ'_{12} follow an anticorrelation. This happens because we have used the condition on λ_{12} and λ'_{12}, i.e., $\lambda_{12} + \lambda'_{12} < 4\pi$ which makes the plot look like this. In particular, if we look at $\lambda_{12} = 4\pi$ then $\lambda'_{12} = 0$ and vice versa and this follows all over the points. In the plots, we have also shown the color variation for each point which represents the scalar sector contribution to muon $(g-2)$. The more green points represent $\lambda'_{12} < 0$ and $\tan\beta$ larger values which corresponds to $M_A < M_{H^\pm}$ and hence contribute in the muon $(g-2)$ more. Additionally, each point also satisfies the condition $\lambda_{12} + \lambda'_{12} > -2\sqrt{\lambda_1\lambda_2}$ which keeps the possibility that their sum can be negative as well and not exactly zero. In the lower panel, we have shown the same plots but for the type-II 2HDM model. Here, one of the main constraints comes from the $b \to s\gamma$ which demand charged Higgs mass $M_{H^\pm} > 800$ GeV. Because of such high values of $M_{H^\pm}$, we also need M_A around that order otherwise $\lambda_{12}, \lambda'_{12}$ would

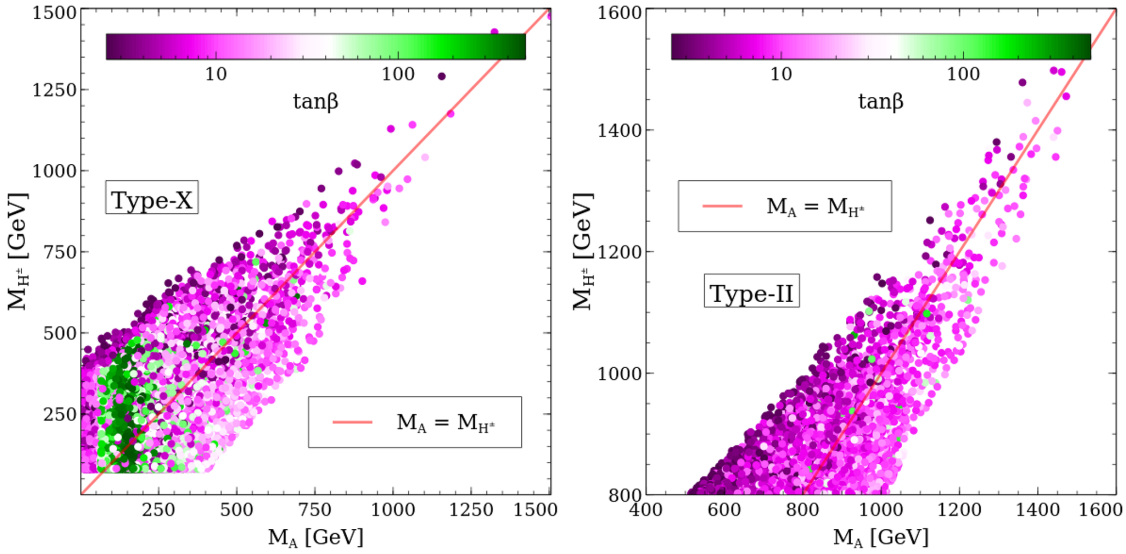

FIG. 4. LP shows the scatter plot in the $M_A - M_{H^\pm}$ plane for type-X 2HDM where the color bar shows the variation with respect to $\tan\beta$. In the RP we have also shown the variation in the same plane with the same color variation but for type-II 2HDM.

violate perturbativity. Because of such a high value of $M_{H^\pm}$, we see a very sharp correlation and the starting value for M_A is around 500 GeV. In the RP of the lower panel, we have shown the scatter plot in the $\lambda_{12} - \lambda'_{12}$ plane and the color bar shows the contribution from the scalar sector in $(g-2)_\mu$. We can see from the color bar that most of the contribution comes from the gauge boson mediated process.

In the LP and RP of Fig. 4, we have shown scatter plots in the $M_A - M_{H^\pm}$ for type-X and type-II 2HDM models and in both plots the color variation shows different values of $\tan\beta$. The allowed region is mostly obtained by the perturbativity and the bound from the below conditions on the quartic couplings. In the misalignment limit and $\alpha_{2,3} \to 0$, the quartic couplings $\lambda_{12}, \lambda'_{12}$ can be expressed in terms of the masses as follows:

$$\lambda_{12} \simeq \frac{2M^2_{H^\pm} - (M^2_A + M^2_{h_1} - M^2_{h_2})}{v^2}, \quad \lambda'_{12} \simeq \frac{2}{v^2}(M^2_A - M^2_{H^\pm}). \tag{56}$$

From the above expressions, we can see that the masses of the scalars cannot be very much apart; otherwise, it will conflict with the perturbativity bound. In Fig. 3 we have shown a sharp correlation between M_A and M_{h_1} which will ensure also a sharp correlation with the charged Higgs mass as seen in both the LP and RP. In the LP for type-X 2HDM, we do not have strong constraints on the charged Higgs mass, hence small mass ranges of M_A and $M_{H^\pm}$ are allowed. The color variation on the points implies the different values of $\tan\beta$. The muon $(g-2)$ depends on $\tan\beta$ and M_A generally as $\frac{\tan^2\beta}{M^2_A}$ as can be seen in Sec. V. So for the higher values of M_A we also need higher values of $\tan\beta$ but we have taken maximum $\tan\beta = 500$. In general, higher values of $\tan\beta$ will impact the λ_1 perturbativity bound and also the Yukawa coupling perturbativity bound for the b quark (τ lepton) for the type-II (type-X) 2HDM model puts an upper bound on $\tan\beta < 206 (\tan\beta < 500)$. In the RP, we have shown it for the type-II 2HDM case and we have strong constraints on the charged Higgs mass from $b \to s\gamma$, i.e., $M_{H^\pm} > 800$ GeV. Therefore, we see the allowed range also starts at higher values of M_A. Therefore, for this case, we do not have a dominant contribution from the scalar sector in $(g-2)$ if a very accidental cancellation does not happen among the masses which makes λ_1 perturbative for higher values of $\tan\beta$ as well. The dependence of type-II and type-X 2HDM models on muon $(g-2)$ will be more clear in the later part.

In the LP and RP of Fig. 5, we have shown scatter plots in the $g' - \tan\beta$ plane where the color bars represent the variation for the CP-odd scalar mass and the gauge boson contribution to muon $(g-2)$ in percentage. Let us first discuss the upper panel which is for the type-X 2HDM model. The general contribution from the Higgs sector to $(g-2)_\mu$ can be parametrized as $\Delta a_\mu^{\rm 2HDM} \propto \frac{\tan^2\beta}{M^2_A}$. As we have seen earlier in Fig. 3, $M_A < 100$ GeV is allowed for smaller values of $\tan\beta$ due to the perturbativity limit on λ_1. As explained before $(g-2)_\mu$ is inversely proportional to the mass square M^2_A and linearly to the square of $\tan\beta$. Therefore, $g' < 4 \times 10^{-4}$ and $\tan\beta < 200$; we do not have any points because $(g-2)_\mu$ cannot be produced sufficiently. Once, we have a sufficient contribution to $g-2$ for the parameter space $60 < M_A$ GeV < 300 and $\tan\beta > 200$, then most of the contribution to $(g-2)_\mu$ anomaly comes from the Higgs sector. On the other hand, when $g' > 4 \times 10^{-4}$ then we can produce the total $g-2$ contribution solely

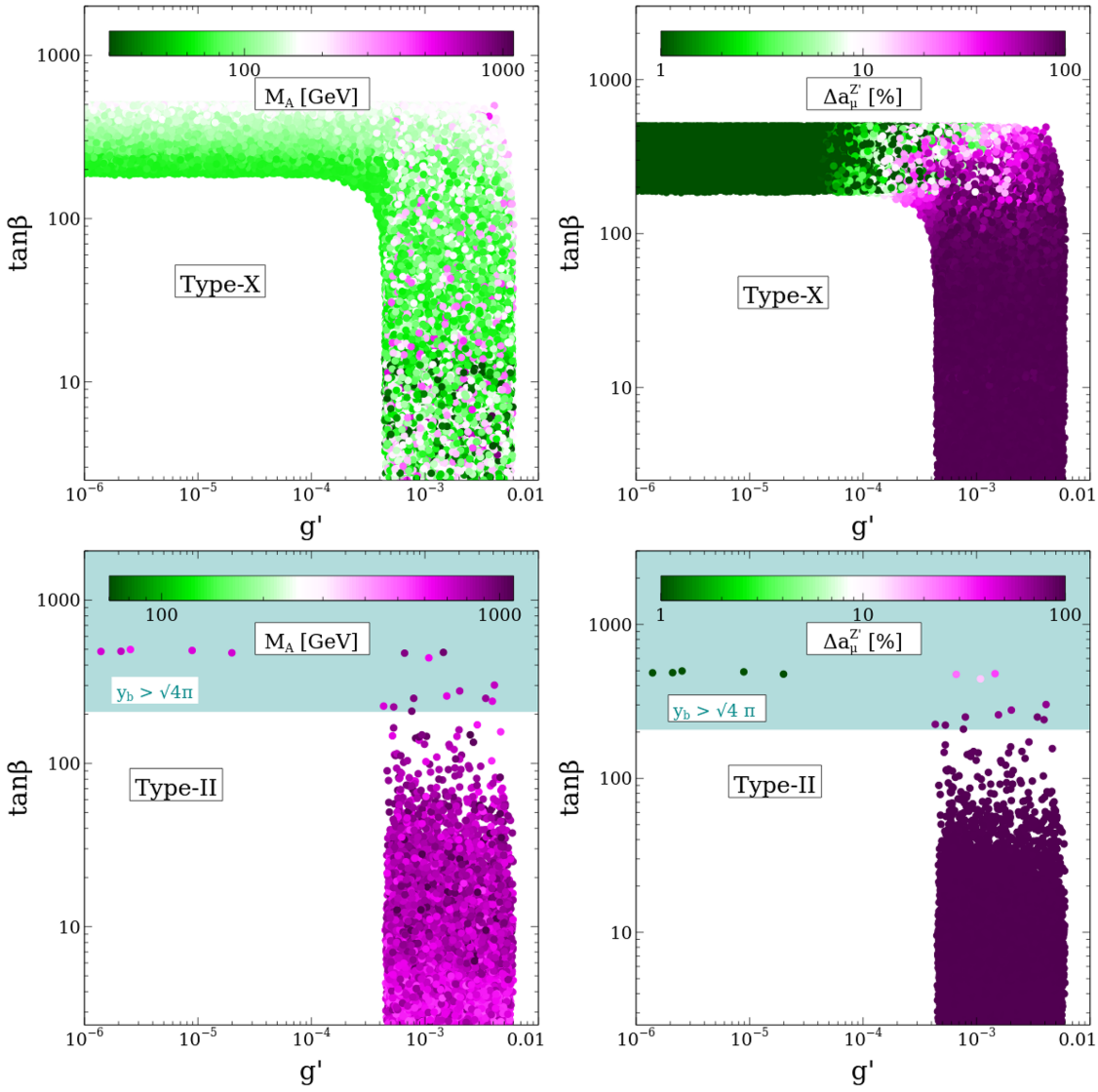

FIG. 5. The LP shows the scatter plot in the $g' - \tan\beta$ plane where the color bar shows the variation with respect to the mass of the CP-odd Higgs A. The RP also shows the variation in the same plane but the color bar represents the Z' contribution to $(g-2)_\mu$.

from the Z', therefore for those parameter spaces lower values of $\tan\beta$ as well as the higher values of M_A are also allowed. On the other hand in the right panel, we have shown the color variation with respect to the $U(1)_X$ gauge boson contribution to $(g-2)_\mu$. As can be seen from Eq. (53), gauge boson contribution to muon $g-2$ is proportional to g'^2. This kind of behavior can be easily seen from the color variation like for $g' < 4 \times 10^{-4}$, the gauge boson contribution is subdominant, but for the opposite regime it is the dominant one. The higher values of g', represented by the region $g' > 6 \times 10^{-3}$, are also ruled out because that region will produce a more positive contribution to muon $(g-2)$ anomaly. The green points represent the dominant contribution from the scalar sector, whereas the magenta points represent the dominant contribution from the gauge boson sector Z'. In the lower panel, we have shown the same kind of plots but for the type-II 2HDM model. Since here we have to obey $M_{H^\pm} > 800$ GeV, then we can see larger values of M_A are allowed due to the perturbativity bound. In the LP, we can see a few points; at lower g' those points correspond to $M_A = M_{h_1}$ and small value of M_{h_3}, then those points can pass the perturbativity bound for a high value of $\tan\beta$ value as well. Therefore, those points can give us a full contribution to muon $(g-2)$ from the scalar sector only; although those points fall in the cyan region which corresponds to the perturbative violation for the b-quark Yukawa coupling. In the RP, we can see the distinction between the points which distinguish the contribution from the scalar and gauge boson sectors. Again the points that represent dominant contribution from the scalar sector are ruled out by the perturbativity bound on the b-quark Yukawa coupling.

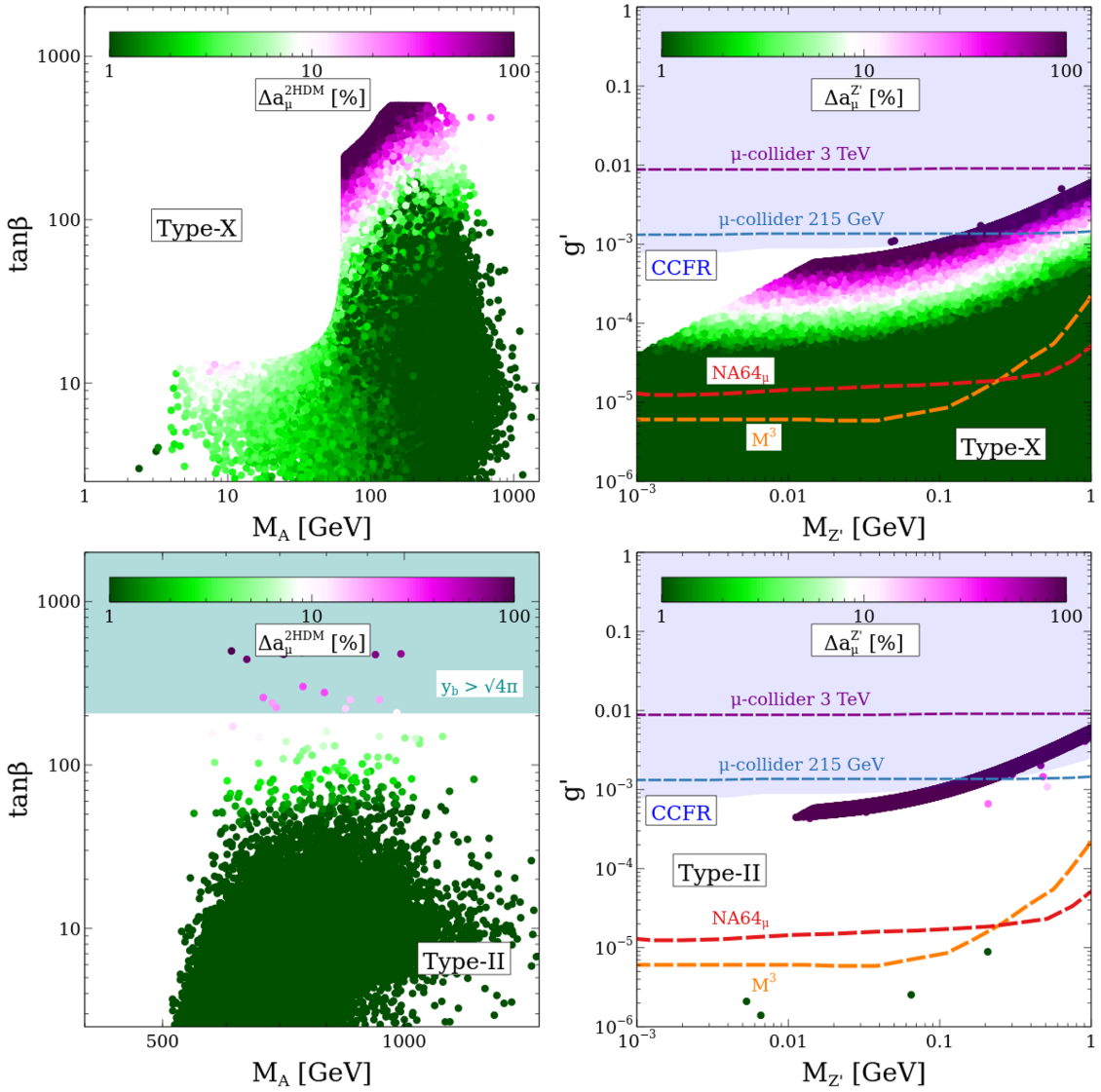

FIG. 6. LP and RP show the scatter plots in the $M_A - \tan\beta$ and $M_{Z'} - g'$ planes, respectively. The color variation in both plots represents the scalar sector contribution and gauge boson contribution to the muon $(g-2)$ in percentage.

In the LP and RP of Fig. 6, we have shown the scatter plots in the $M_A - \tan\beta$ and $M_{Z'} - g'$ planes where the upper panel corresponds to the type-X 2HDM and the lower panel corresponds to the type-II 2HDM model. We first discuss the upper panel, then we discuss the lower panel. As discussed, the LP of Fig. 6 shows the allowed region in the $M_A - \tan\beta$ plane where the color variation represents the Higgs sector contribution to muon $(g-2)$. As can be seen, for $\tan\beta < 60$ the Higgs sector contribution to $(g-2)_\mu$ is less than 10%. Once we go to larger values of $\tan\beta$, say $\tan\beta > 100$, we see the magenta points which represent more than 50% contribution to $(g-2)_\mu$. The color variation in the figure also clearly explains that for a particular value of M_A, if we go for higher values of $\tan\beta$ then we gradually move towards the magenta points, i.e., more contribution to $(g-2)_\mu$ from the Higgs sector. The figure also explains that if one wants the muon $(g-2)$ anomaly is accounted for the Higgs sector, the viable parameter space is very narrow as it is represented only by the deep magenta points. The presence of the extra gauge boson is essential to enlarge the parameter space. We notice, additionally, that the distribution of the points complying with $(g-2)$ has extended for $M_A < 62.5$ as well. These points can conflict with the LHC bound coming from $h_2 \to AA$ decay but needs proper treatment which limits our further discussion. On the other hand in the RP, we have shown the scatter plot in the $M_{Z'} - g'$ plane. Here, the deep magenta region can only explain the $(g-2)_\mu$ anomaly fully if we consider only the gauge boson contribution. But because of the presence of the Higgs

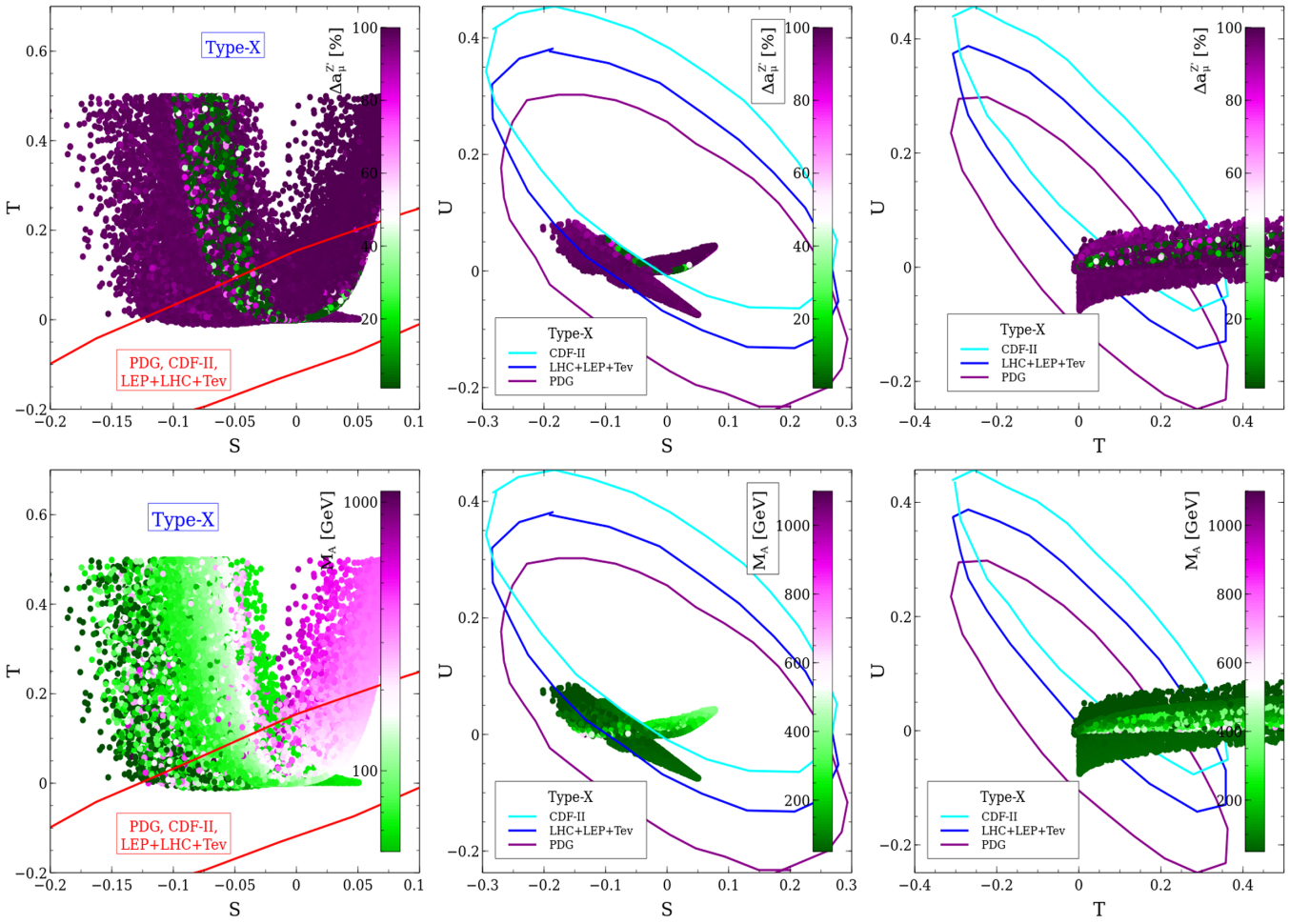

FIG. 7. Scatter plots in $S-T$, $S-U$, and T–U planes after satisfying total DM relic density, muon $(g-2)$, perturbativity, and unitarity bounds. In the upper panel, the color bars show the variation of the Z' contribution to muon $(g-2)$ in percentage whereas the lower panel shows the variation with respect to mass of the CP-odd Higgs A. All of the plots are generated by using a type-X 2HDM kind of model.

sector, the region expands for lower values of g' as well represented by the green points. The region below $M_{Z'} < 0.01$ GeV and $4\times10^{-5} < g' < 8\times10^{-4}$ have no points because those points make $\lambda_{\phi_2} > 4\pi$. A part of the allowed region in the $M_{Z'} - g'$ plane was already explored by the CCFR neutrino trident experiment [111], represented by the blue shaded region in the plot. Moreover, the remaining parameter space will be explored through different experiments like $NA64_\mu$ at CERN [112], M^3 at Fermi Lab [113], and even at the proposed muon collider [114]. All of the future bounds are represented by the dashed lines and labeled according to the associated experiment name. In the lower panel, the figures are in the same plane and also with the same kind of color variation for the type-II 2HDM case. As we have seen before, scalar sector contribution to muon $(g-2)$ is subdominant so the full contribution comes from the gauge boson sector which can be seen from both left and right plots. A few points which can give 100% are the points which satisfy $M_A = M_{h_1}$, and the M_{h_3} value is small near the SM Higgs mass. But those few points are already contradictory due to the perturbative violation of the b-quark Yukawa coupling.

VII. EXPLANATION OF W-BOSON MASS OBSERVED AT CDF-II

Recently, the CDF-II collaboration has reported the larger values of W-boson mass based on their 8.8 fb^{-1} data of $\sqrt{s} = 1.96$ TeV run of $p\bar{p}$ collision. They have obtained the W-boson mass [6],

$$M_W^{\text{CDF-II}} = 80.4335 \pm 0.0094 \text{ GeV} \tag{57}$$

while there is also a prediction for the W-boson mass from other collaborations like LEP [115], ATLAS [116], LHCb [117], and Tevatron [6,118] and can be summarized as

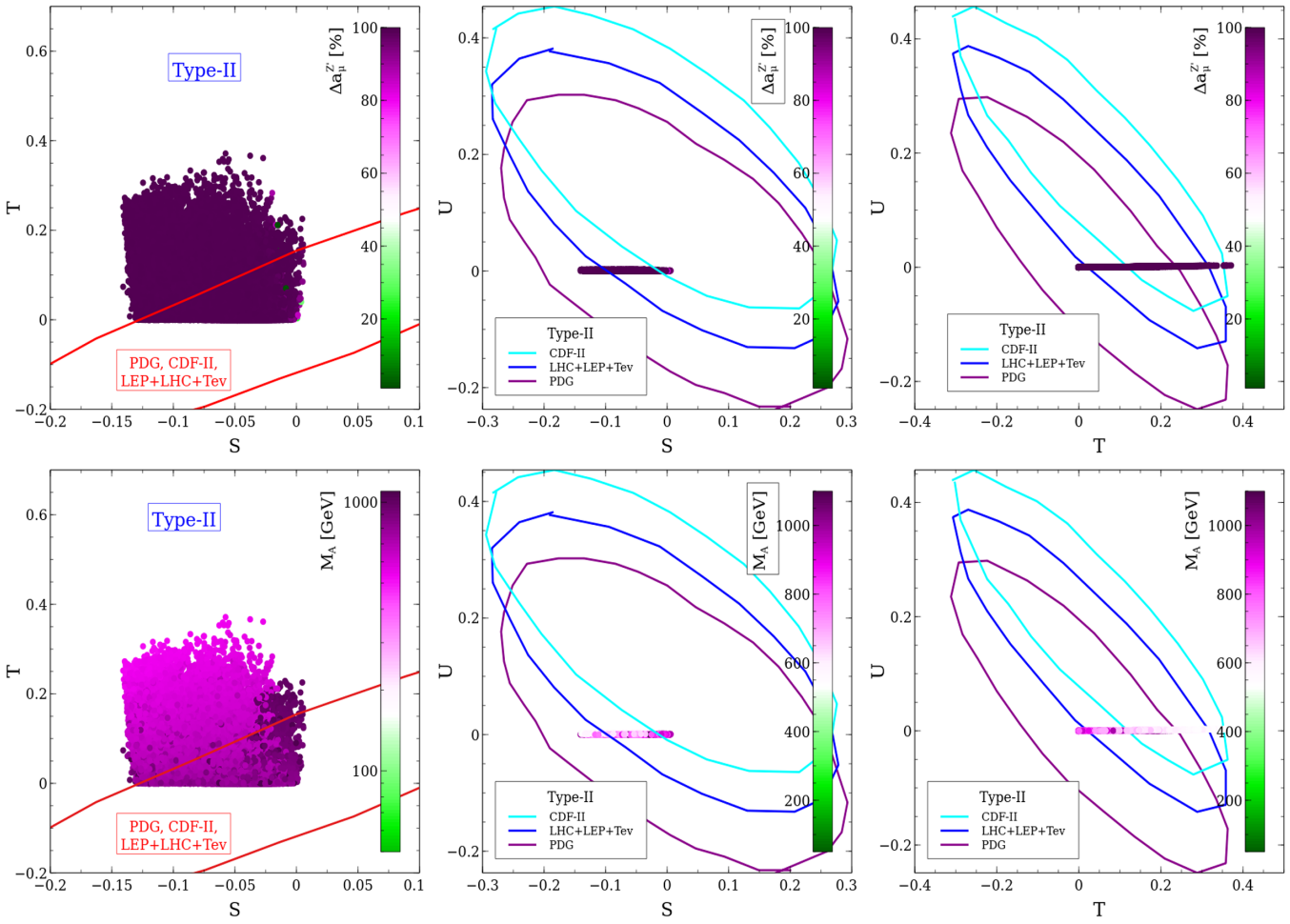

FIG. 8. Scatter plots in $S-T$, $S-U$, and T–U planes after satisfying total DM relic density, muon $(g-2)$, perturbativity, and unitarity bounds. In the upper panel, the color bars show the variation of the Z' contribution to muon $(g-2)$ in percentage whereas the lower panel shows the variation with respect to mass of the CP-odd Higgs A. All of the plots have been generated by using a type-II kind of 2HDM model.

$$M_W = 80.4112 \pm 0.0076\,\text{GeV}, \quad \text{LHC} + \text{LEP} + \text{Tevatron},$$
$$M_W = 80.3790 \pm 0.0120\,\text{GeV}, \quad \text{PDG2020}. \tag{58}$$

The values disagree with each other with quite a high statistical significance as the CDF-II disagrees with the SM values at the significance of 7σ. We need beyond Standard Model contribution to address the increased value of the W-boson mass at the CDF-II detector. The recent reanalysis of ATLAS data collected in 2011 for the 7 TeV run corresponding to 4.6 fb^{-1} integrated luminosity using the state-of-the-art analysis methods estimated the W-boson mass which is in agreement with the SM predicted value [119]. Therefore, it is very early to conclude that the discrepancy observed at the CDF-II measurement is due to the BSM physics; still, investigate the possibility of the present model to explain the discrepancy at CDF-II as well as the SM predicted value. In the present work, we have additional particles which can give extra contributions to the W-boson mass and hence potentially account for the experimental anomaly. In order to investigate quantitatively such possibility, we have calculated the oblique parameters S, T, and U by following Ref. [120] for the present work which also coincides with the result obtained in Refs. [47,48] in the particular limit. The deviation of the mass of the W-boson, with respect to the SM prediction, can be expressed in terms of the oblique parameters as [120]

$$M_W^2 = M_W^2|_{\text{SM}} \times \left[1 + \frac{\alpha}{c_w^2 - s_w^2}\left(-\frac{1}{2}S + c_w^2 T + \frac{c_w^2 - s_w^2}{4 s_w^2} U\right)\right], \tag{59}$$

where $s_w^2 = \sin^2\theta_w \simeq 0.23$ and α is the fine structure constant at the scale of Z-boson pole mass. From the above expression, it is clear that if the oblique parameters S, T, and U are small or zero then the W-boson mass coincides with the SM value.

In Fig. 7, we have shown scatter plots among the oblique parameters plane, namely, $S-T$, $S-U$, and $T-U$ in the context of the type-X 2HDM model. In the upper panel, we

have shown the percentage of gauge boson contribution to $(g-2)_\mu$ whereas in the lower panel, we have shown the color variation in terms of the mass of the CP-odd scalar A. Through these plots, we have tried to show that our model can explain all of the measured values of the W-boson mass from ATLAS to CDF-II. The contour plots in different oblique parameters plane which fit the W-boson mass from different measurements, namely, PDG, CDF-II, and LEP + LHC + Tev, have been borrowed from Ref. [121]. In the first plot of the upper panel we have shown the allowed region in the S–T plane and the red contour plot represents the allowed region to explain the W-boson mass from different measurements. We can see a substantial amount of points within the red contour region. Similarly, we have shown the allowed region in the $S-U$ and T–U planes where the allowed regions from different experimental measurements of W-boson mass are represented as cyan, blue, and magenta contour plots. We can see in both plots we have common overlap regions which can explain the W-boson mass simultaneously from all of the measurements. In generating the plots, we have considered $T < 0.5$ because beyond this value, there will be more contribution to the W-boson mass and have already been ruled out from experiments. In the lower panel, we have shown the color variation in terms of the mass values M_A. We can see that both lower and higher values of M_A can explain the W-boson mass. Finally, in Fig. 8, we have also shown the region which can explain the W-boson mass from the different measurements in the type-II 2HDM model. Here we need higher values of M_A and the other mass scales, so we have less beyond SM effects on the S, T, U parameters which can be easily seen from the figures. All of the points represent a subdominant contribution to $(g-2)_\mu$ from the scalar sector so 100% contribution comes from the gauge sector. The variation of the oblique parameters slightly differs from the SM value which is S, T, $U = 0$.

VIII. SUMMARY AND CONCLUSION

In this work, we have proposed and studied a framework aiming to address some of the most relevant puzzles which call for the existence of physics beyond the Standard Model: dark matter, neutrino masses, $(g-2)_\mu$, and anomalous measure of the W-mass by CDF-II. In this context, we have taken 2HDM as the basis model and extended its particle content by two singlet scalars and three right-handed neutrinos. The gauge group has also been extended by an additional Abelian gauge symmetry. Additionally, we have also introduced an additional global symmetry which can be resembled with the PQ symmetry and upon its breaking we have the axion field. Among the two singlet scalars, one of them is charged under the $U(1)_{L_\mu - L_\tau}$ gauge group and its CP-odd component becomes the longitudinal part of the additional gauge boson and imparts its mass. On the other hand, the remaining CP-odd scalar coming from ϕ_1 becomes an axion field when the global PQ symmetry breaks spontaneously due to ϕ_1 VEV. The axion field can be produced in the early universe by the misalignment mechanism and becomes a cold DM. In the case of type-II configurations for the Yukawa couplings of the scalar sector, the axion DM can be identified with the QCD axion possibly solving the strong CP problem. Even if it cannot account for the solution of the latter puzzle, we have considered, in this work, the type-X scenario as well as it appears to be more favorable for interpreting the $(g-2)$ anomaly and for neutrino masses. Another important beyond SM problem, namely, neutrino mass, can also be addressed by the type-I seesaw mechanism when the scalars take the spontaneous VEV. In particular, few elements in the RH neutrino mass matrix are suppressed by the Planck mass; therefore it is hard to generate the RH neutrino mass above 1 GeV for the type-II 2HDM case but for the type-X case RH neutrino mass can be generated as large as 1 TeV. Although the aforementioned statement is true when we consider all of the elements in the right-handed neutrino mass matrix are the same, they can be deviated by a few orders of magnitude obeying the neutrino oscillation data. We are also able to explain the muon $(g-2)$ anomaly in the present setup. In our work, we have two contributions in the $(g-2)_\mu$, one coming from the scalar sector and the other contribution coming from the additional gauge boson. As found in the case of type-II 2HDM, due to strong constraint on the charge Higgs mass from $b \to s\gamma$ measurement the scalar sector contribution to $(g-2)_\mu$ is negligible but for type-X 2HDM variant scalars can produce 100% deficiency in $(g-2)_\mu$. Therefore, for type-X we can have the freedom to choose gauge coupling and gauge boson mass which can give us higher values of VEV and, hence, the possibility of obtaining TeV scale right-handed neutrinos. The gauge sector effect in Δa_μ is the same irrespective of type-X or type-II variants of the 2HDM model. Additionally, due to the presence of additional particles, we can have an effect on the oblique parameters S, T, U which can contribute to the W-boson mass. We have found that the allowed parameters after taking into account all the observables can also explain the CDF-II measurement in some part of the parameter space and the remaining part can address the SM predicted value, i.e., subdominant BSM contribution. Therefore, our model can explain both the data for the W-boson mass, i.e., CDF-II and SM values of the W-boson mass. Finally, we conclude that our model can explain many beyond Standard Model drawbacks simultaneously namely dark matter, neutrino mass, strong CP problem, muon $(g-2)$, and the potential discrepancy in the measurement of the W-boson mass. Additionally, the present work has the potential to explain the gravitation waves and inflation due to the rich scalar sector which are left to pursue in the future.

ACKNOWLEDGMENTS

S. K. extends sincere thanks for the warm hospitality provided at the Department of Mathematical and Computer Sciences, Physical Sciences, and Earth Sciences, University of Messina, during the visit when this project was initiated. S. K. acknowledges Laura Covi for useful discussions. This work used the Scientific Computing Cluster at GWDG, the joint data center of Max Planck Society for the Advancement of Science (MPG) and University of Göttingen.

APPENDIX A: GAUGE ANOMALY

Gauge anomaly conditions associated with the gauge symmetry are very crucial to make them zero, otherwise the theory would become nonrenormalizable. For a generator T^a of any gauge symmetry, the gauge anomaly term can be written as

$$\partial^\mu J^a_\mu = \left(\sum_{\text{left}} A(R_l) - \sum_{\text{right}} A(R_r)\right) \frac{g^2}{128\pi^2} \text{Tr}[T^a\{T^b, T^c\}] F\tilde{F}, \tag{A1}$$

where $A(R)$ depends on the group representation; for fundamental representation it is equal to $A(R)|_{\text{funda}} = 1$ and for adjoint or singlet representation is $A(R)|_{\text{Adj or sin}\, g} = 0$. In SM, the left-handed fermions are in fundamental representation whereas right-handed fermions are in singlet representation; therefore, in the present work we mainly need to check the quantity $\text{Tr}[T^a\{T^b, T^c\}]$ if it vanishes or not for all possible combinations of the gauge groups. It is clear that if the trace contains only one non-Abelian generator then it trivially vanishes because of the traceless property of the non-Abelian generator. Moreover, due to the vectorial nature of the fermions under $U(1)_{L_\mu - L_\tau}$ gauge symmetry, the gauge combinations $[SU(3)]^2 \times U(1)_{L_\mu - L_\tau}$, $[U(1)_{L_\mu - L_\tau}]^2 \times U(1)_Y$, $[U(1)_{L_\mu - L_\tau}]^3$, and $[\text{Gravity}]^2 \times U(1)_{L_\mu - L_\tau}$ vanish. The nonzero contributions include

$$[SU(2)]^2 \times U(1)_{L_\mu - L_\tau}: \frac{\text{Tr}[\sigma^a\sigma^b]}{2} \sum_{i=1}^{3} (3b_i + b'_i)$$
$$U(1)_Y^2 \times U(1)_{L_\mu - L_\tau}: \sum_{i=1}^{3} \left(-\frac{3}{2} b_i - \frac{1}{2} b'_i\right). \tag{A2}$$

Nonzero contributions can be made zero by choosing

$$\sum_{i=1}^{3} (3b_i + b'_i) = 0. \tag{A3}$$

Therefore, there are many ways we can choose b_i, b'_i $(i = 1, 2, 2)$ to satisfy the above equation. In this work, we have chosen the simplest combination which is $b_i = 0$, $b'_1 = 0$, and $b'_2 = -b'_3 = 1$ which is $U(1)_{L_\mu - L_\tau}$ Abelian extension of the SM and has been extensively studied in the literature. The more general kind of $U(1)$ gauge symmetry with different kinds of flavor combinations has been shown in [122].

APPENDIX B: BOUND ON THE QUARTIC COUPLINGS

(i) *Bound from below.* In this part, we put the bound on the quartic couplings which are needed to prevent the total potential from becoming negative for very high values of the fields. In this part, we have assumed that $\lambda_{H_1\phi_1}, \lambda_{H_2\phi_1}, \lambda_{\phi_1\phi_2} \sim 0$. As described in [123], we can have two scenarios depending on $\lambda'_{12} > 0$ or < 0.

Case I. $\lambda'_{12} > 0$.

$$\Omega_1 = \left(\lambda_{\phi_2}, \lambda_1, \lambda_2 \geq 0; \lambda_{H_i\phi_2} > -2\sqrt{\lambda_{\phi_2}\lambda_i}; \lambda_{12} > -2\sqrt{\lambda_1\lambda_2}; \lambda_{H_1\phi_2} \geq -\lambda_{H_2\phi_2}\sqrt{\frac{\lambda_1}{\lambda_2}}\right)$$
$$\bigcup \left(\lambda_{\phi_2}, \lambda_1, \lambda_2 > 0; 2\sqrt{\lambda_{\phi_2}\lambda_2} \geq \lambda_{H_2\phi_2} > -2\sqrt{\lambda_{\phi_2}\lambda_2}; -\lambda_{H_2\phi_2}\sqrt{\frac{\lambda_1}{\lambda_2}} \geq \lambda_{H_1\phi_2} > -2\sqrt{\lambda_{\phi_2}\lambda_1};\right.$$
$$\left. 2\lambda_{\phi_2}\lambda_{12} > \lambda_{H_1\phi_2}\lambda_{H_2\phi_2} - \sqrt{(\lambda^2_{H_1\phi_2} - 4\lambda_{\phi_2}\lambda_1)(\lambda^2_{H_2\phi_2} - 4\lambda_{\phi_2}\lambda_2)}\right), \tag{B1}$$

where $i = 1, 2$.

Case II. $\lambda'_{12} < 0$. For this case, the condition will be the same as before but we need to replace 12 by $\lambda_{12} + \lambda'_{12}$, i.e., $\Omega_2 = \Omega_1|_{\lambda_{12} \to \lambda_{12} + \lambda'_{12}}$.

(ii) *Bound from perturbativity.* The quartic couplings can be written in terms of the scalar masses and mixing angles in the following manner:

$$\begin{aligned}
\lambda_1 &= \frac{1}{2v_1^2}\left(\frac{\mu v_2 v_{\phi_1}}{\sqrt{2}v_1} + \sum_{i=1}^{3} R_{i1}^2 M_{h_i}^2\right)\\
\lambda_2 &= \frac{1}{2v_2^2}\left(\frac{\mu v_1 v_{\phi_1}}{\sqrt{2}v_2} + \sum_{i=1}^{3} R_{i2}^2 M_{h_i}^2\right)\\
\lambda_{\phi_2} &= \frac{1}{2v_{\phi_2}^2}\sum_{i=1}^{3} R_{i3}^2 M_{h_i}^2\\
\lambda_{12} &= \frac{2M_{H^\pm}^2}{v^2} + \frac{\mu v_{\phi_1}}{\sqrt{2}v_1 v_2} + \frac{1}{v_1 v_2}\sum_{i=1}^{3} R_{i1}R_{i2}M_{h_i}^2\\
\lambda'_{12} &= -\frac{2M_{H^\pm}^2}{v^2} + \frac{2M_A^2}{(v^2 + \frac{v_1^2 v_2^2}{v_{\phi_1}^2})}\\
\lambda_{H_1\phi_2} &= \frac{1}{v_1 v_{\phi_2}}\sum_{i=1}^{3} R_{i1}R_{i3}M_{h_i}^2\\
\lambda_{H_2\phi_2} &= \frac{1}{v_2 v_{\phi_2}}\sum_{i=1}^{3} R_{i2}R_{i3}M_{h_i}^2. \qquad \text{(B2)}
\end{aligned}$$

APPENDIX C: OBLIQUE PARAMETERS *S*, *T*, AND *U*

By following Ref. [120], we can write down the scalars in terms of the mass eigenstates when the first component in the lhs column matrix matches with the SM Higgs neutral component as

$$\begin{pmatrix} \phi_a + iG \\ \phi_b + iA \\ \phi_c + ia \\ \phi_d \end{pmatrix} = \begin{pmatrix} i & V_{11} & V_{12} & V_{13} & 0 & U_{13} & 0 \\ 0 & V_{21} & V_{22} & V_{23} & i & U_{23} & 0 \\ 0 & V_{31} & V_{32} & V_{33} & 0 & U_{33} & i \\ 0 & R_{13} & R_{23} & R_{33} & 0 & 0 & 0 \end{pmatrix} \begin{pmatrix} G \\ h_1 \\ h_2 \\ h_3 \\ A \\ \phi_1 \\ a \end{pmatrix}, \qquad \text{(C1)}$$

where

$$\begin{aligned}
&V_{11} = U_{11}R_{11} + U_{12}R_{12}, \quad V_{12} = U_{11}R_{21} + U_{12}R_{22}, \quad V_{13} = U_{11}R_{31} + U_{12}R_{32},\\
&V_{21} = U_{21}R_{11} + U_{22}R_{12}, \quad V_{22} = U_{21}R_{21} + U_{22}R_{22}, \quad V_{23} = U_{21}R_{31} + U_{22}R_{32},\\
&V_{31} = U_{31}R_{11} + U_{32}R_{12}, \quad V_{32} = U_{31}R_{21} + U_{32}R_{22}, \quad V_{33} = U_{31}R_{31} + U_{32}R_{32}. \qquad \text{(C2)}
\end{aligned}$$

In the above relations, R_{ij} and U_{ij} are matrices which diagonalize the *CP*-even and *CP*-odd mass matrices shown in Eqs. (10) and (16). The oblique parameters S, T, and U can be expressed as

$$\begin{aligned}
S = \frac{1}{24\pi}\big[&(2s_w^2-1)^2 G(M_{H^\pm}^2, M_{H^\pm}^2, M_Z^2) + (V_{21}^2 G(M_{h_1}^2, M_A^2, M_Z^2) + V_{22}^2 G(M_{h_2}^2, M_A^2, M_Z^2)\\
&+ V_{23}^2 G(M_{h_3}^2, M_A^2, M_Z^2) + U_{23}^2 G(M_A^2, M_{\phi_1}^2, M_Z^2)) - 2\ln M_{H^\pm}^2 + ((V_{11}^2 + V_{21}^2)\ln M_{h_1}^2\\
&+ (V_{12}^2 + V_{22}^2)\ln M_{h_2}^2 + (V_{13}^2 + V_{23}^2)\ln M_{h_3}^2 + \ln M_A^2 + (U_{13}^2 + U_{23}^2)\ln M_{\phi_1}^2) - \ln M_{h_{\rm SM}}^2\\
&(V_{11}^2 \hat{G}(M_{h_1}^2, M_Z^2) + V_{12}^2 \hat{G}(M_{h_2}^2, M_Z^2) + V_{13}^2 \hat{G}(M_{h_3}^2, M_Z^2) + U_{13}^2 \hat{G}(M_{\phi_1}^2, M_Z^2) - \hat{G}(M_{h_{\rm SM}}^2, M_Z^2))\big] \qquad \text{(C3)}
\end{aligned}$$

$$\begin{aligned}
T = \frac{1}{16\pi^2 M_W^2 s_W^2}\big[&(V_{21}^2 F(M_{H^\pm}^2, M_{h_1}^2) + V_{22}^2 F(M_{H^\pm}^2, M_{h_2}^2) + V_{23}^2 F(M_{H^\pm}^2, M_{h_3}^2) + F(M_{H^\pm}^2, M_A^2)\\
&+ U_{23}^2 F(M_{H^\pm}^2, M_{\phi_1}^2)) - (V_{21}^2 F(M_{h_1}^2, M_A^2) + V_{22}^2 F(M_{h_2}^2, M_A^2) + V_{23}^2 F(M_{h_3}^2, M_A^2)\\
&+ U_{23}^2 F(M_A^2, M_{\phi_1}^2)) + 3(V_{11}^2 (F(M_Z^2, M_{h_1}^2) - F(M_W^2, M_{h_1}^2)) + V_{12}^2 (F(M_Z^2, M_{h_2}^2) - F(M_W^2, M_{h_2}^2))\\
&+ V_{13}^2 (F(M_Z^2, M_{h_3}^2) - F(M_W^2, M_{h_3}^2)) + U_{13}^2 (F(M_Z^2, M_{\phi_1}^2) - F(M_W^2, M_{\phi_1}^2))\\
&- (F(M_Z^2, M_{h_{\rm SM}}^2) - F(M_W^2, M_{h_{\rm SM}}^2)))\big] \qquad \text{(C4)}
\end{aligned}$$

$$
\begin{aligned}
U = \frac{1}{24\pi}\big[&(V_{21}^2 G(M_{H^\pm}^2, M_{h_1}^2, M_W^2) + V_{22}^2 G(M_{H^\pm}^2, M_{h_2}^2, M_W^2) + V_{23}^2 G(M_{H^\pm}^2, M_{h_3}^2, M_W^2) \\
&+ G(M_{H^\pm}^2, M_A^2, M_W^2) + U_{23}^2 G(M_{H^\pm}^2, M_{\phi_1}^2, M_W^2) - (2s_W^2 - 1)^2 G(M_{H^\pm}^2, M_{H^\pm}^2, M_Z^2)) \\
&- (V_{21}^2 G(M_{h_1}^2, M_A^2, M_Z^2) + V_{22}^2 G(M_{h_2}^2, M_A^2, M_Z^2) + V_{23}^2 G(M_{h_3}^2, M_A^2, M_Z^2) + U_{23}^2 G(M_A^2, M_{\phi_1}^2, M_Z^2)) \\
&+ (V_{11}^2 (\hat{G}(M_{h_1}^2, M_W^2) - \hat{G}(M_{h_1}^2, M_Z^2)) + V_{12}^2 (\hat{G}(M_{h_2}^2, M_W^2) - \hat{G}(M_{h_2}^2, M_Z^2)) \\
&+ V_{13}^2 (\hat{G}(M_{h_3}^2, M_W^2) - \hat{G}(M_{h_3}^2, M_Z^2)) + U_{13}^2 (\hat{G}(M_{\phi_1}^2, M_W^2) - \hat{G}(M_{\phi_1}^2, M_Z^2)) \\
&- (\hat{G}(M_{h_{\rm SM}}^2, M_W^2) - \hat{G}(M_{h_{\rm SM}}^2, M_Z^2)))\big].
\end{aligned} \tag{C5}
$$

The explicit form of the functions $F(x,y)$, $G(x,y,z)$, and $\hat{G}(x,z)$ are given by

$$
\begin{aligned}
F(x,y) &= \begin{cases} \frac{x+y}{2} - \frac{xy}{x-y}\ln\frac{x}{y}, & \text{for } x \neq y \\ 0, & \text{for } x = y \end{cases} \\
G(x,y,z) &= \begin{cases} -\frac{16}{3} + 5\frac{x+y}{z} - 2\frac{(x-y)^2}{z^2} + \frac{3}{z}\left[\frac{x^2+y^2}{x-y} - \frac{x^2-y^2}{z} + \frac{(x-y)^3}{3z^2}\right]\ln\frac{x}{y} + \frac{r}{z^3}f(p,q), & \text{for } x \neq y \\ -\frac{16}{3} + \frac{16}{z}x + \frac{r}{z^3}f(p,q), & \text{for } x = y \end{cases} \\
\hat{G}(x,z) &= -\frac{79}{3} + 9\frac{x}{z} - 2\frac{x^2}{z^2} + \left(-10 + 18\frac{x}{z} - 6\frac{x^2}{z^2} + \frac{x^3}{z^3} - 9\frac{x+z}{x-z}\right)\ln\frac{x}{z} \\
&\quad + \left(12 - 4\frac{x}{z} + \frac{x^2}{z^2}\right)\frac{f(x, x^2-4xz)}{z},
\end{aligned} \tag{C6}
$$

where $p = x + y - z$, $q = z^2 - 2z(x+y) + (x-y)^2$, and the function $f(p,q)$ can be expressed as

$$
f(p,q) = \begin{cases} \sqrt{q}\ln\left|\frac{p-\sqrt{q}}{p+\sqrt{q}}\right|, & \text{for } q \neq 0 \\ 0, & \text{for } q = 0 \\ 2\sqrt{-q}\tan^{-1}\frac{\sqrt{-q}}{p}, & \text{for } q < 0. \end{cases}
$$

[1] G. Bertone and D. Hooper, Rev. Mod. Phys. **90**, 045002 (2018).
[2] T. Kajita, Rev. Mod. Phys. **88**, 030501 (2016).
[3] A. B. McDonald, Rev. Mod. Phys. **88**, 030502 (2016).
[4] I. Esteban, M. C. Gonzalez-Garcia, M. Maltoni, T. Schwetz, and A. Zhou, J. High Energy Phys. 09 (2020) 178.
[5] T. Aoyama, N. Asmussen, M. Benayoun, J. Bijnens, T. Blum, M. Bruno, I. Caprini, C. M. Carloni Calame, M. Cè, G. Colangelo *et al.*, Phys. Rep. **887**, 1 (2020).
[6] T. Aaltonen *et al.* (CDF Collaboration), Science **376**, 170 (2022).
[7] Y. Sofue and V. Rubin, Annu. Rev. Astron. Astrophys. **39**, 137 (2001).
[8] D. Clowe, A. Gonzalez, and M. Markevitch, Astrophys. J. **604**, 596 (2004).
[9] N. Aghanim *et al.* (Planck Collaboration), Astron. Astrophys. **641**, A6 (2020); **652**, C4(E) (2021).
[10] C. A. Baker, D. D. Doyle, P. Geltenbort, K. Green, M. G. D. van der Grinten, P. G. Harris, P. Iaydjiev, S. N. Ivanov, D. J. R. May, J. M. Pendlebury *et al.*, Phys. Rev. Lett. **97**, 131801 (2006).
[11] R. D. Peccei and H. R. Quinn, Phys. Rev. Lett. **38**, 1440 (1977).
[12] R. D. Peccei and H. R. Quinn, Phys. Rev. D **16**, 1791 (1977).
[13] S. Weinberg, Phys. Rev. Lett. **40**, 223 (1978).
[14] F. Wilczek, Phys. Rev. Lett. **40**, 279 (1978).
[15] Y. Fukuda *et al.* (Super-Kamiokande Collaboration), Phys. Rev. Lett. **81**, 1562 (1998).
[16] Q. R. Ahmad *et al.* (SNO Collaboration), Phys. Rev. Lett. **89**, 011301 (2002).

[17] K. Eguchi *et al.* (KamLAND Collaboration), Phys. Rev. Lett. **90**, 021802 (2003).
[18] F. P. An *et al.* (Daya Bay Collaboration), Phys. Rev. Lett. **116**, 061801 (2016); **118**, 099902(E) (2017).
[19] B. Abi *et al.* (Muon $g-2$ Collaboration), Phys. Rev. Lett. **126**, 141801 (2021).
[20] S. Borsanyi, Z. Fodor, J. N. Guenther, C. Hoelbling, S. D. Katz, L. Lellouch, T. Lippert, K. Miura, L. Parato, K. K. Szabo *et al.*, Nature (London) **593**, 51 (2021).
[21] F. V. Ignatov *et al.* (CMD-3 Collaboration), arXiv:2302.08834.
[22] S. L. Glashow and S. Weinberg, Phys. Rev. D **15**, 1958 (1977).
[23] E. A. Paschos, Phys. Rev. D **15**, 1966 (1977).
[24] F. Björkeroth, E. J. Chun, and S. F. King, Phys. Lett. B **777**, 428 (2018).
[25] K. Harigaya, M. Ibe, K. Schmitz, and T. T. Yanagida, Phys. Rev. D **88**, 075022 (2013).
[26] A. G. Dias, V. Pleitez, and M. D. Tonasse, Phys. Rev. D **69**, 015007 (2004).
[27] Y. H. Ahn, Phys. Rev. D **91**, 056005 (2015).
[28] G. Honecker and W. Staessens, J. Phys. Conf. Ser. **631**, 012080 (2015).
[29] T. Hur, H. S. Lee, and C. Luhn, J. High Energy Phys. 01 (2009) 081.
[30] J. D. Clarke and R. R. Volkas, Phys. Rev. D **93**, 035001 (2016).
[31] S. W. Hawking, Phys. Lett. B **195**, 337 (1987).
[32] G. V. Lavrelashvili, V. A. Rubakov, and P. G. Tinyakov, JETP Lett. **46**, 167 (1987).
[33] S. B. Giddings and A. Strominger, Nucl. Phys. **B307**, 854 (1988).
[34] S. R. Coleman, Nucl. Phys. **B310**, 643 (1988).
[35] G. Gilbert, Nucl. Phys. **B328**, 159 (1989).
[36] A. G. Dias, J. Leite, and D. S. V. Gonçalves, Phys. Rev. D **104**, 075014 (2021).
[37] Y. Amhis *et al.* (HFLAV Collaboration), Eur. Phys. J. C **77**, 895 (2017).
[38] M. Misiak and M. Steinhauser, Eur. Phys. J. C **77**, 201 (2017).
[39] A. R. Zhitnitsky, Sov. J. Nucl. Phys. **31**, 260 (1980).
[40] M. Dine, W. Fischler, and M. Srednicki, Phys. Lett. **104B**, 199 (1981).
[41] J. H. Chang, R. Essig, and S. D. McDermott, J. High Energy Phys. 09 (2018) 051.
[42] G. C. Branco, P. M. Ferreira, L. Lavoura, M. N. Rebelo, M. Sher, and J. P. Silva, Phys. Rep. **516**, 1 (2012).
[43] J. Preskill, M. B. Wise, and F. Wilczek, Phys. Lett. **120B**, 127 (1983).
[44] L. F. Abbott and P. Sikivie, Phys. Lett. **120B**, 133 (1983).
[45] M. Dine and W. Fischler, Phys. Lett. **120B**, 137 (1983).
[46] L. Di Luzio, M. Giannotti, E. Nardi, and L. Visinelli, Phys. Rep. **870**, 1 (2020).
[47] M. Muhlleitner, M. O. P. Sampaio, R. Santos, and J. Wittbrodt, J. High Energy Phys. 03 (2017) 094.
[48] A. Arhrib, R. Benbrik, M. El Kacimi, L. Rahili, and S. Semlali, Eur. Phys. J. C **80**, 13 (2020).
[49] Z. Maki, M. Nakagawa, and S. Sakata, Prog. Theor. Phys. **28**, 870 (1962).
[50] C. Jarlskog, Phys. Rev. Lett. **55**, 1039 (1985).
[51] A. Biswas, S. Choubey, and S. Khan, J. High Energy Phys. 09 (2016) 147.
[52] F. F. Deppisch, P. S. Bhupal Dev, and A. Pilaftsis, New J. Phys. **17**, 075019 (2015).
[53] D. Gorbunov and M. Shaposhnikov, J. High Energy Phys. 10 (2007) 015; 11 (2013) 101(E).
[54] A. Boyarsky, O. Ruchayskiy, and M. Shaposhnikov, Annu. Rev. Nucl. Part. Sci. **59**, 191 (2009).
[55] O. Ruchayskiy and A. Ivashko, J. Cosmol. Astropart. Phys. 10 (2012) 014.
[56] V. Domcke, M. Drewes, M. Hufnagel, and M. Lucente, J. High Energy Phys. 01 (2021) 200.
[57] R. Foot, A. Kobakhidze, K. L. McDonald, and R. R. Volkas, Phys. Rev. D **89**, 115018 (2014).
[58] J. E. Kim, Phys. Rev. Lett. **43**, 103 (1979).
[59] M. A. Shifman, A. I. Vainshtein, and V. I. Zakharov, Nucl. Phys. **B166**, 493 (1980).
[60] L. Covi and S. Khan, J. Cosmol. Astropart. Phys. 09 (2022) 064.
[61] M. S. Turner, Phys. Rev. D **33**, 889 (1986).
[62] D. J. E. Marsh, Phys. Rep. **643**, 1 (2016).
[63] G. Grilli di Cortona, E. Hardy, J. Pardo Vega, and G. Villadoro, J. High Energy Phys. 01 (2016) 034.
[64] M. Gorghetto, E. Hardy, and G. Villadoro, J. High Energy Phys. 07 (2018) 151.
[65] M. Buschmann, J. W. Foster, and B. R. Safdi, Phys. Rev. Lett. **124**, 161103 (2020).
[66] M. Gorghetto, E. Hardy, and G. Villadoro, SciPost Phys. **10**, 050 (2021).
[67] M. Buschmann, J. W. Foster, A. Hook, A. Peterson, D. E. Willcox, W. Zhang, and B. R. Safdi, Nat. Commun. **13**, 1049 (2022).
[68] L. Caloni, M. Gerbino, M. Lattanzi, and L. Visinelli, J. Cosmol. Astropart. Phys. 09 (2022) 021.
[69] M. Kawasaki and K. Nakayama, Annu. Rev. Nucl. Part. Sci. **63**, 69 (2013).
[70] M. Kawasaki, E. Sonomoto, and T. T. Yanagida, Phys. Lett. B **782**, 181 (2018).
[71] P. A. R. Ade *et al.* (Planck Collaboration), Astron. Astrophys. **594**, A20 (2016).
[72] Y. Akrami *et al.* (Planck Collaboration), Astron. Astrophys. **641**, A10 (2020).
[73] P. A. R. Ade *et al.* (Planck Collaboration), Astron. Astrophys. **594**, A13 (2016).
[74] N. Du *et al.* (ADMX Collaboration), Phys. Rev. Lett. **120**, 151301 (2018).
[75] T. Braine *et al.* (ADMX Collaboration), Phys. Rev. Lett. **124**, 101303 (2020).
[76] C. Bartram *et al.* (ADMX Collaboration), Phys. Rev. Lett. **127**, 261803 (2021).
[77] S. Lee, S. Ahn, J. Choi, B. Rok Ko, and Y. K. Semertzidis, *Proc. Sci.*, EPS-HEP2019 (2020) 101 [arXiv:1910.00047].
[78] Y. K. Semertzidis, J. E. Kim, S. Youn, J. Choi, W. Chung, S. Haciomeroglu, D. Kim, J. Kim, B. Ko, O. Kwon *et al.*, arXiv:1910.11591.
[79] P. Brun *et al.* (MADMAX Collaboration), Eur. Phys. J. C **79**, 186 (2019).
[80] D. Alesini, D. Babusci, P. Beltrame S. J., F. Björkeroth, F. Bossi, P. Ciambrone, G. Delle Monache, D. Di Gioacchino, P. Falferi, A. Gallo *et al.*, arXiv:1911.02427.

[81] J. L. Ouellet, C. P. Salemi, J. W. Foster, R. Henning, Z. Bogorad, J. M. Conrad, J. A. Formaggio, Y. Kahn, J. Minervini, A. Radovinsky *et al.*, Phys. Rev. Lett. **122**, 121802 (2019).
[82] G. Charpak, F. J. M. Farley, and R. L. Garwin, Phys. Lett. **1**, 16 (1962).
[83] G. Charpak, P. J. M. Farley, E. L. Garwin, T. Muller, J. C. Sens, and A. Zichichi, Nuovo Cimento **37**, 1241 (1965).
[84] F. Combley and E. Picasso, Phys. Rep. **14**, 1 (1974).
[85] J. Bailey *et al.* (CERN-Mainz-Daresbury Collaboration), Nucl. Phys. **B150**, 1 (1979).
[86] G. W. Bennett *et al.* (Muon $g-2$ Collaboration), Phys. Rev. D **73**, 072003 (2006).
[87] M. Davier, A. Hoecker, B. Malaescu, and Z. Zhang, Eur. Phys. J. C **77**, 827 (2017).
[88] A. Keshavarzi, D. Nomura, and T. Teubner, Phys. Rev. D **97**, 114025 (2018).
[89] G. Colangelo, M. Hoferichter, and P. Stoffer, J. High Energy Phys. 02 (2019) 006.
[90] M. Davier, A. Hoecker, B. Malaescu, and Z. Zhang, Eur. Phys. J. C **80**, 241 (2020); **80**, 410(E) (2020).
[91] G. Arcadi, N. Benincasa, A. Djouadi, and K. Kannike, Phys. Rev. D **108**, 055010 (2023).
[92] G. Arcadi and A. Djouadi, Phys. Rev. D **106**, 095008 (2022).
[93] G. Arcadi, A. Djouadi, and F. d. Queiroz, Phys. Lett. B **834**, 137436 (2022).
[94] G. Arcadi, Á. S. de Jesus, T. B. de Melo, F. S. Queiroz, and Y. S. Villamizar, Nucl. Phys. **B982**, 115882 (2022).
[95] E. J. Chun and J. Kim, J. High Energy Phys. 07 (2016) 110.
[96] A. Biswas, S. Choubey, and S. Khan, J. High Energy Phys. 02 (2017) 123.
[97] A. Biswas, S. Choubey, L. Covi, and S. Khan, J. Cosmol. Astropart. Phys. 02 (2018) 002.
[98] A. Biswas and S. Khan, J. High Energy Phys. 07 (2022) 037.
[99] F. Costa, S. Khan, and J. Kim, J. High Energy Phys. 06 (2022) 026.
[100] B. e. Lautrup, A. Peterman, and E. de Rafael, Phys. Rep. **3**, 193 (1972).
[101] J. P. Leveille, Nucl. Phys. **B137**, 63 (1978).
[102] A. Dedes and H. E. Haber, J. High Energy Phys. 05 (2001) 006.
[103] A. Broggio, E. J. Chun, M. Passera, K. M. Patel, and S. K. Vempati, J. High Energy Phys. 11 (2014) 058.
[104] V. Ilisie, J. High Energy Phys. 04 (2015) 077.
[105] D. Chang, W. F. Chang, C. H. Chou, and W. Y. Keung, Phys. Rev. D **63**, 091301 (2001).
[106] K. m. Cheung, C. H. Chou, and O. C. W. Kong, Phys. Rev. D **64**, 111301 (2001).
[107] K. Cheung and O. C. W. Kong, Phys. Rev. D **68**, 053003 (2003).
[108] S. N. Gninenko and N. V. Krasnikov, Phys. Lett. B **513**, 119 (2001).
[109] S. Baek, N. G. Deshpande, X. G. He, and P. Ko, Phys. Rev. D **64**, 055006 (2001).
[110] M. Misiak, H. M. Asatrian, R. Boughezal, M. Czakon, T. Ewerth, A. Ferroglia, P. Fiedler, P. Gambino, C. Greub, U. Haisch *et al.*, Phys. Rev. Lett. **114**, 221801 (2015).
[111] W. Altmannshofer, S. Gori, M. Pospelov, and I. Yavin, Phys. Rev. Lett. **113**, 091801 (2014).
[112] S. N. Gninenko, N. V. Krasnikov, and V. A. Matveev, Phys. Rev. D **91**, 095015 (2015).
[113] Y. Kahn, G. Krnjaic, N. Tran, and A. Whitbeck, J. High Energy Phys. 09 (2018) 153.
[114] J. de Blas *et al.* (Muon Collider Collaboration), arXiv:2203.07261.
[115] T. A. Aaltonen *et al.* (CDF and D0 Collaborations), Phys. Rev. D **88**, 052018 (2013).
[116] M. Aaboud *et al.* (ATLAS Collaboration), Eur. Phys. J. C **78**, 110 (2018); **78**, 898(E) (2018).
[117] R. Aaij *et al.* (LHCb Collaboration), J. High Energy Phys. 01 (2022) 036.
[118] T. A. Aaltonen *et al.* (CDF Collaboration), Phys. Rev. D **89**, 072003 (2014).
[119] ATLAS Collaboration, Improved W boson mass measurement using 7 TeV proton-proton collisions with the ATLAS detector, Report No. ATLAS-CONF-2023-004.
[120] W. Grimus, L. Lavoura, O. M. Ogreid, and P. Osland, Nucl. Phys. **B801**, 81 (2008).
[121] P. Asadi, C. Cesarotti, K. Fraser, S. Homiller, and A. Parikh, Phys. Rev. D **108**, 055026 (2023).
[122] C. Kownacki, E. Ma, N. Pollard, and M. Zakeri, Phys. Lett. B **766**, 149 (2017).
[123] K. G. Klimenko, Theor. Math. Phys. **62**, 58 (1985).